MASTER

# An antenna for the base station of the median demonstrator

Khusial, S.

*Award date:*
1996

7404

EINDHOVEN UNIVERSITY OF TECHNOLOGY
FACULTY OF ELECTRICAL ENGINEERING
TELECOMMUNICATIONS DIVISION

# *AN ANTENNA FOR THE BASE STATION OF THE MEDIAN DEMONSTRATOR*

by: S. Khusial

Report of graduation work,
performed from September 1995 to June 1996

Supervisor: prof. dr. ir. G. Brussaard
Mentors: dr. ir. M.H.A.J. Herben
dr. ir. P.F.M. Smulders

# *Abstract*

This thesis treats the design of an antenna intended for operation at the base station of a broadband wireless LAN demonstrator. This demonstrator will be developed in the framework of the ACTS project MEDIAN (Wireless Broadband Customer Premises Network/Local Area Network for Professional and Residential Multimedia Applications). The applied frequency band is 62-63 GHz.

According to MEDIAN specifications, the antenna has to radiate downwards and it has to provide a circular footprint at 3 metress below. The diameter of this coverage plane-section should be 8 metress.

Two antenna types have been investigated, viz: the bended biconical-horn antenna and the shaped reflector antenna.

Analysis of the radiation pattern of the bended biconical-horn antenna yields an unacceptable fluctuation of the fieldstrength in the coverage plane-section of many dB's. Therefore, this option can be ruled out for our application.

On the contrary, analysis of the shaped reflector antenna on the basis of Geometrical Optics and Uniform Theory of Diffraction yields promising results; the reflector with a diameter of only 30 centimetres could be shaped so that the spatial fluctuation of the fieldstrength remains below 0.5 dB in the coverage plane-section whereas outside this coverage plane-section the fieldstrength falls off very rapidly.

# *Table of Contents*

# *Acronyms and Symbols*

Acronyms

| | |
|---|---|
| ACTS | Advanced Communications Technologies and Services |
| AGV | Autonomous Guided Vehicles |
| EEC | Equivalent Edge Current Calculation |
| GTD | Geometrical Theory of Diffraction |
| IMST | Institut fuer Mobil- und Satellitenfunktechnik |
| ISB | Incident Shadow Boundary |
| LAN | Local Area Network |
| MSS | Median Server Station |
| MPS | Median Portable Station |
| RSB | Reflection Shadow Boundary |
| UTD | Uniform Geometrical Theory of Diffraction |

Symbols

| | |
|---|---|
| $A$ | Width of the horn aperture of the biconical-horn antenna [m] |
| $A_0$ | Constant for the far-field of a Huygens feed [V] |
| $A(s_i^i, s_i^d)$ | Caustic divergence factor |
| $a$ | Spacing distance between upper and lower part of the biconical-horn antenna [m] |
| $b$ | Diameter of the radial section of the biconical and bended biconical-horn antenna [m] |
| $C(x)$, $S(x)$ | Fresnel integrals |
| $D$ | Diameter of the shaped reflector [m] |
| $D_c$ | Diameter of the coverage plane-section [m] |
| $\vec{D}$ | Dyadic diffraction coefficient |
| $D_h$ | Scalar diffraction coefficient for the hard boundary condition |
| $D_s$ | Scalar diffraction coefficient for the soft boundary condition |
| $D(\theta,s)$ | Directivity of the biconical-horn antenna |
| $D(\theta',s)$ | Directivity of the bended biconical-horn antenna |
| $d$ | Distance from the central point to another point of the coverage plane-section [m] |
| $d_i$ | Interior diameter of the circular waveguide of the biconical-horn antenna [m] |
| $E$ | Electric field on the coverage plane-section [V/m] |

| | |
|---|---|
| $E_{dB}$ | Electric field on coverage plane-section relative to power radiated by the feed [dB] |
| $E_{\%\ ripple}$ | Deviation (ripple) in the electric field on the coverage plane-section [%] |
| $E^{d1}(x_c)$ | Diffracted field on the coverage plane-section at $x_c$ from the upper point [V/m] |
| $E^{d2}(x_c)$ | Diffracted field on the coverage plane-section at $x_c$ from the lower point [V/m] |
| $E^{r}(x_c)$ | Reflected field on the coverage plane-section at $x_c$ [V/m] |
| $E_{tot}(x_c)$ | Total electric field on the coverage plane-section at $x_c$ [V/m] |
| $\vec{E}^{i}(Q_i)$ | Incident electric field at point $Q_i$ [V/m] |
| $E^{d}(P)$ | Diffracted field due to the diffraction point $Q_i$ [V/m] |
| $E_\theta$ | Total electric field in θ-direction [V/m] |
| $E_\phi^d$ | Diffraction field from diffraction point $Q_i$ in ϕ-direction [V/m] |
| $E_\theta^d$ | Diffraction field from diffraction point $Q_i$ in θ-direction [V/m] |
| $E_{\beta_0}^d$ | Diffracted field parallel to the plane of diffraction [V/m] |
| $E_{\phi_0}^d$ | Diffracted field perpendicular to the plane of diffraction [V/m] |
| $E_{\beta_0}^i$ | Incident field parallel to the plane of incidence [V/m] |
| $E_{\phi_0}^i$ | Incident field perpendicular to the plane of incidence [V/m] |
| $E_{f\phi}^i$ | Incident field from the feed in ϕ-direction [V/m] |
| $E_{f\theta}^i$ | Incident field from the feed in θ-direction [V/m] |
| $F$ | Distance between the feed and the origin of $(x_r,y_r)$ coordinate system [m] |
| $F(z)$ | Modified Fresnel Transition function |
| $F(\theta,s)$ | Structure function of the gain for the biconical-horn antenna |
| $F(\theta',s)$ | Structure function of the gain for the bended biconical-horn antenna |
| $G_a(\theta)$ | Gain function of the biconical-horn antenna |
| $G_f(\psi)$ | Gain function of the feed |
| $H(r)$ | Illumination function of the coverage plane-section [$W/m^2$] |
| $k$ | Wave number [$m^{-1}$] |
| $L$ | Length of the horn of the biconical and bended biconical-horn antenna [m] |
| $L_a$ | Antenna loss [dB] |
| $L_m$ | Antenna loss due to impedance mismatch [dB] |
| $L^i$, $L^r$ | Distance parameters for the modified Fresnel Transition function [m] |
| $\ell$ | Propagation path in the horn of the biconical and bended biconical-horn antenna [m] |
| $n$ | Positive real in the power of the cosine of the gain function of the feed |
| $\vec{n}$ | Unit vector normal to the edge at $Q_i$ and directed away from the centre of curvature |
| $\vec{n}_{refl}$ | Normal unit vector to the reflector surface at $Q_i$ |
| $p_1$ | Relative power on coverage plane-section |

| | |
|---|---|
| $p_2$ | Relative power radiated by the feed |
| $P_{center}$ | Power at the centre of the reflector [W] |
| $P_{edge}$ | Power at the edge of the reflector [W] |
| $P_f$ | Power radiated by the feed [W] |
| $P_r(r, \theta, s)$ | Power received by the MPS antenna (transmitted by the biconical-horn) [W] |
| $P_r(r, \theta', s)$ | Power received by the MPS antenna (transmitted by the bended biconical-horn) [W] |
| $P_t$ | Total power radiated by the MSS antenna or the feed [W] |
| $Q_i$ | Diffraction points (i=1, 2) |
| $r$ | Distance from the antenna to the observation point [m] |
| $r_1, r_2$ | Boundaries of the Fresnel integrals for the biconical and bended biconical-horn antenna |
| $r^d$ | Angle between the diffraction ray and reflector surface tangent, which is perpendicular to the plane of diffraction [degrees] |
| $r^i$ | Angle between the incident ray and reflector surface tangent, which is perpendicular to the plane of incidence [degrees] |
| $s$ | Phase error on the aperture of the biconical and bended biconical-horn antenna |
| $\vec{S}$ | Powerflux flowing through a surface |
| $\vec{s}_i^{\,i}$ | Unit vector in the direction of the incident ray |
| $\vec{s}_i^{\,d}$ | Unit vector in the direction of the diffracted ray |
| $s_1^d$ | Distance from the upper diffraction point to the observation point [m] |
| $s_2^d$ | Distance from the lower diffraction point to the observation point [m] |
| $\vec{T}$ | Unit vector tangent to the edge at $Q_i$ |
| $U_\alpha$ | Constant for the far-field of a Huygens feed |
| $V(x_c)$ | Voltage at the terminals of the isotropic antenna in the observation point |
| $(x_c,y_c)$ | A coordinate point of the coverage plane-section |
| $(x_r,y_r)$ | A coordinate point of the reflector |
| $(x_s,y_s)$ | Intersection point of the reflected ray through the edge with the reflected ray that lies very close to it |
| $Z_0$ | Intrinsic impedance of free space [Ω] |
| $\alpha$ | Maximum angle between the horizontal axis and the ray from the feed [degrees] |
| $\beta$ | Angle of bending of the bended biconical-horn antenna [degrees] |
| $\beta_0$ | Angle between $\vec{s}_i^{\,i}$ and the tangent $\vec{T}$ to the edge at the point of diffraction [degrees] |
| $\vec{\beta}_0^{\,i}$ | Unit vector parallel to the incident plane |
| $\vec{\beta}_0^{\,d}$ | Unit vector parallel to the diffraction plane |
| $\Delta h$ | Height of the MSS antenna [m] |

| | |
|---|---|
| $\delta$ | Angle between the tangent in $Q_i$ along the reflector surface and the unit vector normal to the edge at $Q_i$ [degrees] |
| $\varepsilon_{rel}$ | Relative error between the power radiated by the feed and the power on the coverage plane-section |
| $\gamma$ | Coverage angle from the MSS antenna [degrees] |
| $\vec{\phi}_0^{\,i}$ | Unit vector perpendicular to the incident plane |
| $\vec{\phi}_0^{\,d}$ | Unit vector perpendicular to the diffraction plane |
| $\lambda$ | Wavelength [m] |
| $\mu_i$ | Angle between the horizontal plane and the diffracted rays (i=1,2) [degrees] |
| $\mu_3$ | Angle between the horizontal plane and the reflected ray [degrees] |
| $\theta$ | Elevation angle [degrees] |
| $\theta'$ | Real elevation angle of bended biconical-horn antenna [degrees] |
| $\rho_1^i$ , $\rho_2^i$ | Principal radii of curvature of the incident wavefront at $Q_i$ [m] |
| $\rho_1^r$ , $\rho_2^r$ | Principal radii of curvature of the reflected wavefront at $Q_i$ [m] |
| $\rho_c$ | Distance between the caustic at the edge and the second caustic of diffracted rays [m] |
| $\rho^i$ | Ray length from the feed to the reflector [m] |
| $\rho_0$ | Maximum ray length from the feed to the reflector [m] |
| $\rho^r$ | Length of the reflected ray [m] |
| $\rho_{max}^r$ | Maximum length of the reflected ray [m] |
| $\rho_g$ | Radius of the curvature of the edge at the diffraction point [m] |
| $\rho_e^i$ | Radius of curvature of the incident wavefront at the edge, fixed plane of incidence which contains the unit vectors $\vec{s}_i^{\,i}$ and the unit vector $\vec{T}$ tangent to the edge at $Q_i$ [m] |
| $\Psi^i$ | Angle between the horizontal axis and the ray from the feed [degrees] |
| $\Psi^r$ | Angle between the horizontal axis and the reflected ray [degrees] |
| $\Psi_{max}^r$ | Maximum angle between the horizontal axis and the reflected ray [degrees] |

# 1. General introduction

## 1.1 Introduction

Indoor radio LANs operating in the millimetre (mm) frequency range may offer a large information transport capacity and sharply defined cell boundaries [1]. The use of mm-wave frequencies enables the creation of high traffic/user density cells, in case the boundaries of an indoor pico-cell (cell radius < 100 m) are formed by walls and floors consisting of 'hard' materials, like concrete and steel through which mm-waves cannot propagate. Radio coverage within a pico-cell can be controlled and optimized by appropriately dimensioning the applied antennas.

From 1995, the Telecommunications Division of the Eindhoven University of Technology participates in the ACTS project MEDIAN (Wireless Broadband Customer Premises Network/Local Area Network for Professional and Residential Multimedia Applications) initiated and managed by IMST[1]. One of the objectives of this project is to evaluate and optimize the performance of a wireless LAN, suitable for multimedia applications. Furthermore, a demonstrator system should be implemented for examination and demonstration of the concept. This system will consist of one base station and two (wireless) portable stations. The transmission of information between the portable stations will take place via the base station. The system will be tested in various user environments. Characteristics that distinguish the MEDIAN concept from conventional wireless LAN's are the unprecedented aggregate transport capacity (totally up to 150 Mbits/s) and the applied frequency band (62-63) GHz.

Typical applications are broadband cableless LAN's in which the portable stations are essentially fixed during operation but also broadband vehicular applications like cableless cameras in TV-studios and Autonomous Guided Vehicles (AGV) in factories.

The Telecommunications Division is responsible for the design and manufacturing of the antennas to be used in the MEDIAN demonstrator system. This graduation thesis treats the design of the base station
antenna as well as the portable station antennas. The objective is to achieve a more-or-less uniform coverage in a pre-defined coverage area.

This report contains six chapters. In this chapter some requirements of the Median demonstrator are given. Chapter 2 contains a short description of the standard biconical horn antenna. This description serves as a starting point from which the design of a more sophisticated horn antenna, namely the bended biconical horn antenna, can be derived. In Chapter 3, the bended biconical horn antenna is treated. A design of a reflector antenna is described in Chapter 4. Chapter 5 deals with the calculation of the electric field on the coverage area. Chapter 6 deals with the design of a shaped reflector dimensioned on an extended coverage area and the calculation of its shape and the realized field distribution over the coverage area.

[1] Institut fuer Mobil- und Satellitenfunktechnik, Kamp Lintfort, Germany

# 1.2 *Demands of the Median demonstrator scenario*

The MEDIAN demonstrator has to cope with a very stringent linkbudget. Therefore, it is likely that the coverage area will be limited to dimensions in the order of a few metress at maximum. Consequently, antennas must be designed for the MSS (Median Server Station) that uniformly illuminate the plane-section of the coverage area in which each MPS (Median Portable Station) antenna is supposed to be present.

According to proposed Median scenarios the antenna of the base station is fixed on a height of 3 metre from the coverage plane-section whereas the coverage is more or less constant within a circular surface plane-section with a diameter of 8 metre and outside there is no coverage. A sketch of this is depicted in Fig. 1.1. The antennas of the portable stations in the coverage plane-section will now considered to be isotropic antennas and the carrier frequency is $f = 60$ *GHz*.

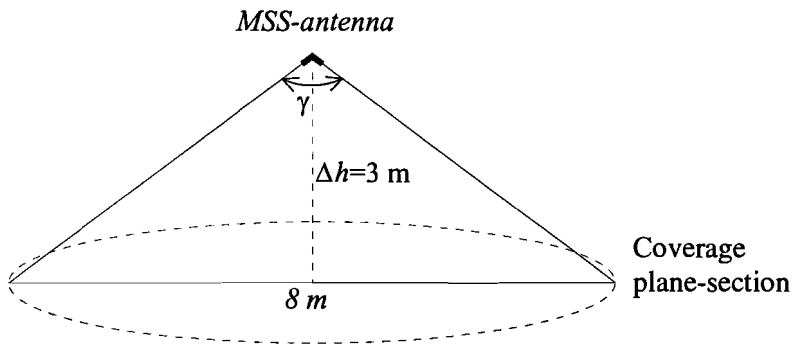


*Fig. 1.1: Coverage area within a circle with a diameter of 8 meter*

The maximum coverage angle '$\gamma$' is: $\gamma = 2.\arctan(4/3) = 106\ °$

This coverage may be achieved in several ways. Three types of aperture antennas will be investigated for possible application as the MSS antenna, viz:

1. **Tilted-beam biconical-horn antenna** for a ring-shaped coverage
2. **Reflector antenna** for uniform coverage
3. **Corrugated-horn antenna** for uniform coverage

In the next sections the tilted-beam biconical-horn antenna and the reflector antenna are discussed.

# 2. *Uniform coverage with biconical-horn antenna*

## 2.1 *Introduction*

Uniform coverage in an indoor pico-cell can be obtained by compensating path loss by antenna gain. The principle is illustrated, schematically in Figure 2.1[1]. This figure shows a typical layout of an indoor radio network consisting of a Median Server Station (MSS) with its antenna located in the middle of the indoor area and two Median Portable Stations (MPS1 and MPS2). All antennas exhibit an omnidirectional pattern in the azimuth plane and an approximately figure-eight-shaped beam in the elevation plane.

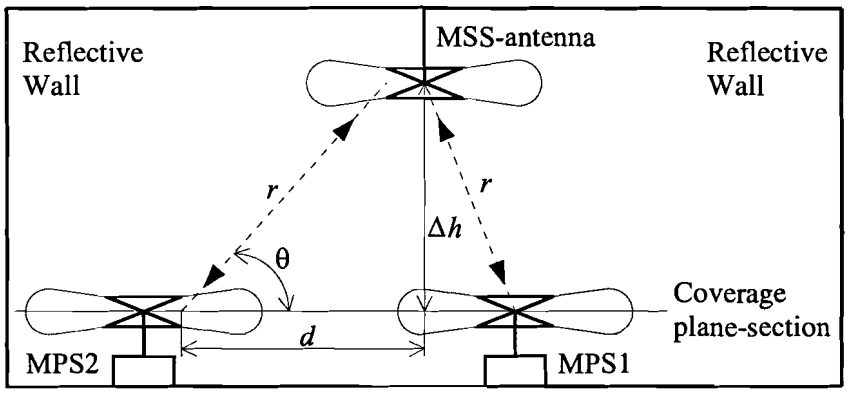


*Fig. 2.1: Layout of indoor radio network*

If a portable station is located in the vicinity of the MSS-antenna such as MPS1, then the direct ray will not only experience a low path loss, but also a small antenna gain. If a portable station is located at a relatively large distance from the MSS-antenna like MPS2, then the direct ray suffers a relatively high path loss, but both antennas exhibit a higher antenna gain. This indicates that path loss and antenna gain may compensate each other to some degree resulting in a more-or-less uniform coverage.

## 2.2 *Biconical-horn antenna*

Figure 2.2 shows [3] a cross-section of a biconical horn antenna. The antenna consists of a radial section, i.e., the spacing between the lower antenna part and upper antenna part with spacing distance $a$ and diameter $b$, a circular waveguide with interior diameter $d_i$ and a biconical horn. The horn has an aperture width $A$ and a length $L$ which is measured from the (virtual) horn apex in the radial section to the centre of the aperture. The taper transforms the incoming linear $TE_{01}$ mode into $TE_{11}$ mode. The circular waveguide contains a polarizer which transforms the $TE_{11}$ mode into two perpendicularly directed waves which are mutually 90° out of phase, thus resulting in a circularly polarized wave.

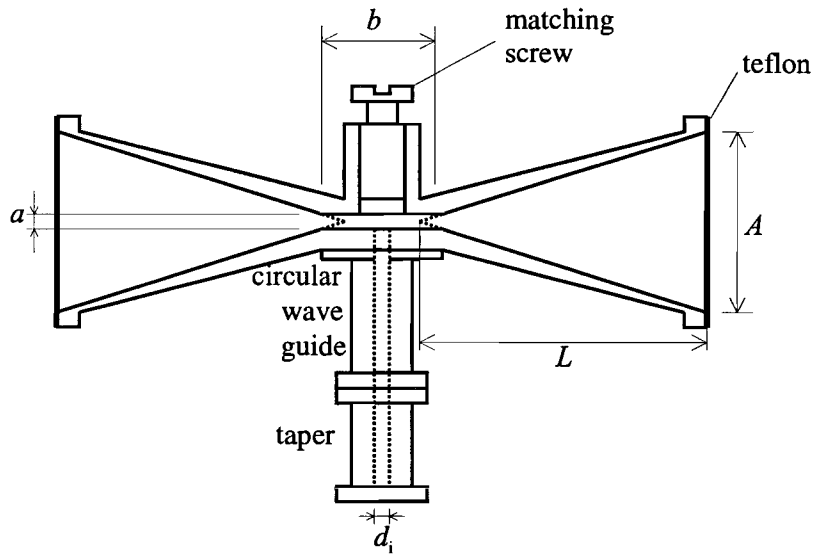


*Fig 2.2: Cross-section of the biconical-horn antenna*

Since the radial line is excited with a circularly polarized wave, the biconical horn exhibits an omnidirectional radiation pattern in the azimuth plane. Hence, the antenna gain function solely depends on the elevation angle θ (see Fig. 2.1). For a good omnidirectional radiation pattern, the launched wave is vertically polarized. For this, we have to take $a < ½\lambda$, otherwise undesirable modes will propagate in the radial section. The radiation pattern is determined by the horn dimensions $A$ and $L$. The propagation path $\ell$ from the horn apex to the horn aperture increases towards the horn edges, so the aperture plane is not a equiphase plane. The phase variation in the aperture plane is given by $\exp[-j2\pi(\ell-L)/\lambda]$. This is similar to the aperture phase distribution in the E-plane of an E-plane sectorial horn antenna with aperture width $A$ and length $L$. The radiation pattern in the elevation plane can therefore be calculated by the method described for sectorial horns with the corresponding mode which is the $TE_{01}$ mode in that case.

## 2.3 *Achievement of near uniform coverage*

The normalized magnitude of the electric field in the elevation plane is equal to

$$|F(\theta,s)| = \frac{|E(\theta)|}{|E(0)|} = \frac{1+\cos\theta}{2}\left[\frac{\left[C(r_2)-C(r_1)\right]^2+\left[S(r_2)-S(r_1)\right]^2}{4\left[C^2\left(2\sqrt{s}\right)+S^2\left(2\sqrt{s}\right)\right]}\right]^{1/2}, \tag{2.1}$$

where $C(x)$ en $S(x)$ are the Fresnel integrals [3]. These integrals are given as

$$C(x)=\int_0^x \cos\left(\frac{\pi}{2}t^2\right)dt\,, \qquad S(x)=\int_0^x \sin\left(\frac{\pi}{2}t^2\right)dt \tag{2.2a}$$

and

$$r_1 = 2\sqrt{s}\left[-1-\frac{1}{4s}\left(\frac{A}{\lambda}\sin\theta\right)\right], \qquad r_2 = 2\sqrt{s}\left[1-\frac{1}{4s}\left(\frac{A}{\lambda}\sin\theta\right)\right]. \tag{2.2b}$$

From Fig. 2.1 it follows that

$$\sin\theta = \frac{\Delta h}{r}\,. \tag{2.3}$$

The parameter $s$ represents the phase error on the antenna aperture and is equal to

$$s = \frac{1}{8}\left(\frac{A}{\lambda}\right)^2 \frac{1}{L/\lambda}\,. \tag{2.4}$$

The directivity $D(\theta,s)$ of the biconical horn antenna can be obtained by

$$D(\theta,s) = \frac{4\pi}{\int_0^{2\pi}\int_{-\pi/2}^{\pi/2} |F(\theta)|^2 \cos\theta \; d\theta \, d\varphi}\,. \tag{2.5}$$

The following equation can be written for the antenna gain function $G_a(\theta)$

$$G_a(\theta) = L_a L_m D(\theta,s)\,|F(\theta)|^2\,. \tag{2.6}$$

where $L_a$ and $L_m$ in (2.6) represent the antenna losses and the impedance mismatches, respectively.

Using the well-known 'radio equation' for the **direct ray** [5], the power received by the remote stations is equal to

$$P_r(r,\theta,s) = G_a^2(\theta)\left(\frac{\lambda}{4\pi r}\right)^2 P_t \ , \tag{2.7}$$

with $P_t$ the total power radiated by the MSS antenna.

The gain of the transmit and receive antenna are equal. The received power is equal to

$$P_r(r,\theta,s) \propto D^2(\theta,s)\,|F(\theta)|^4\left[\frac{\lambda}{4\pi r}\right]^2 . \tag{2.8}$$

Fig. 2.3 shows curves of relative received power against the product of the antenna-dimension parameter $\lambda/A$ and antenna-distance/height-difference ratio $r/\Delta h$ for different values of $s$ relative to the no phase error case ($s$=0, the aperture is a equiphase plane). These curves are normalized to the maximum value for $s$= 0.5.

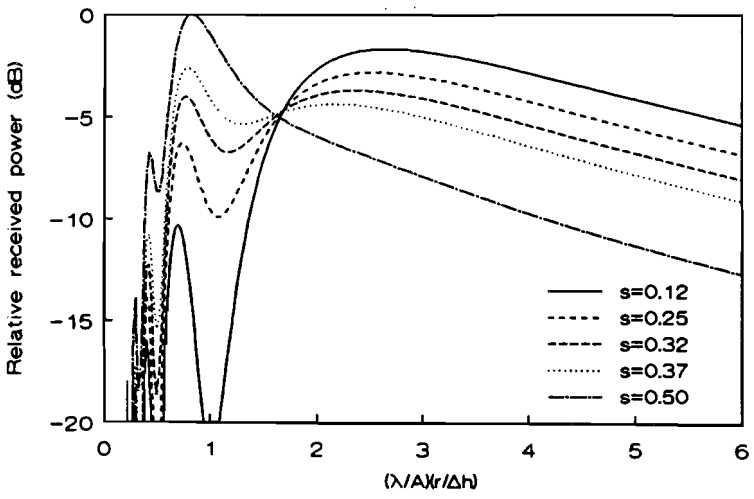


*Fig. 2.3: Universal coverage curves*

The curve with $s$= 0.32 has the optimum performance because a near uniform coverage is achieved with only about 3 dB variation [2] in the received power in the region $0.6 < (\lambda/A)(r/\Delta h) < 5$. Considering the curve of $s$= 0.32 (Fig. 2.3), the minimum value is $(\lambda/A)(r/\Delta h)$= 0.6 [2]. Hence, $r$= 10.8 m for $\Delta h$= 3 m and $A/\lambda$= 6. The horizontal distance on the coverage plane-section (see Fig. 2.1) is equal to

$$d = \sqrt{r^2 - (\Delta h)^2} = 10.4\,m\,.$$

This means that there is almost no coverage for $d$ < 10.4 m on the coverage plane-section. Actually, the biconical-horn antenna exhibits a ring-shaped coverage instead of near uniform coverage.

# 3. Coverage of bended biconical-horn antenna

## 3.1 Bended biconical-horn antenna

The cross-section of the bended biconical-horn antenna is depicted in Fig. 3.1. The bended biconical-horn antenna is achieved by bending the upper antenna part and the lower antenna part of the biconical-horn antenna towards the circular waveguide.

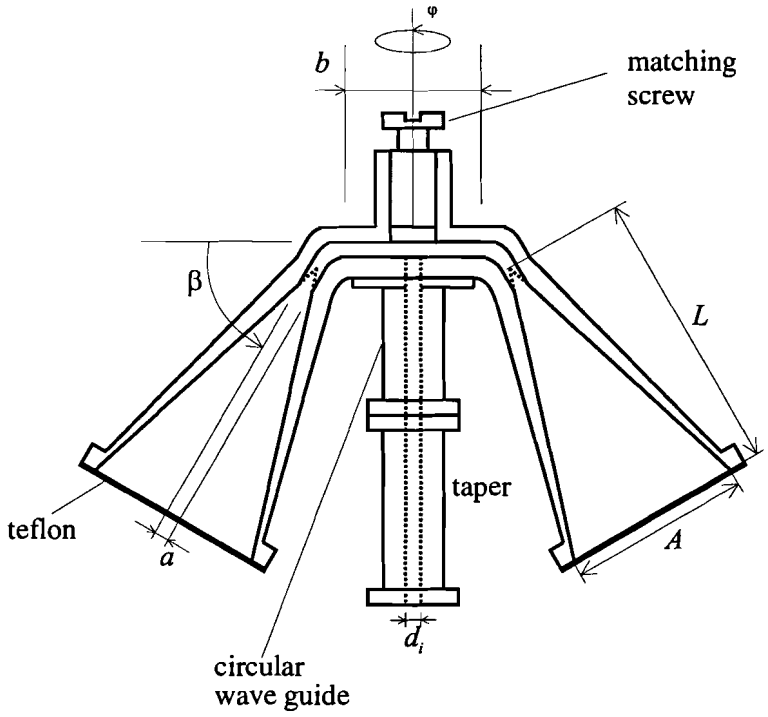


*Fig. 3.1: Cross-section of the bended biconical-horn antenna*

The diameter $b$ of the radial section can be larger than that of standard biconical-horn antenna. The horn has an aperture width $A$ and a length $L$. The incoming linear $TE_{01}$ mode is transformed by the taper into the $TE_{11}$ mode. The circular waveguide contains a polarizer which transforms the linear polarized $TE_{11}$ mode into two perpendicularly directed waves which are mutually 90° out of phase, resulting in a circularly polarized wave. Since the radial line is excited with a circularly polarized wave, the bended biconical-horn antenna exhibits an φ-independent ring-shaped radiation pattern directed to the ground. The spacing distance between the upper and lower antenna part $a < ½\lambda$ is in this case also valid for a good radiation pattern. The radiation pattern is determined by the horn dimensions $A$, $L$ and the angle of bending '$\beta$'. The phase variation is given by $\exp[-j2\pi(\ell-L)/\lambda]$, with $\ell$ being the propagation path in the horn.

# 3.2 *Achievement of ring-shaped coverage area*

The biconical horn antenna shown in Fig. 3.2 must be bent in such a way that the field distribution in the coverage plane-section within a circle with a diameter of 8 metre is about constant whereas outside this area, the field is about zero. To achieve the required coverage, a suitable value for the angle of bending '$\beta$' must be chosen.

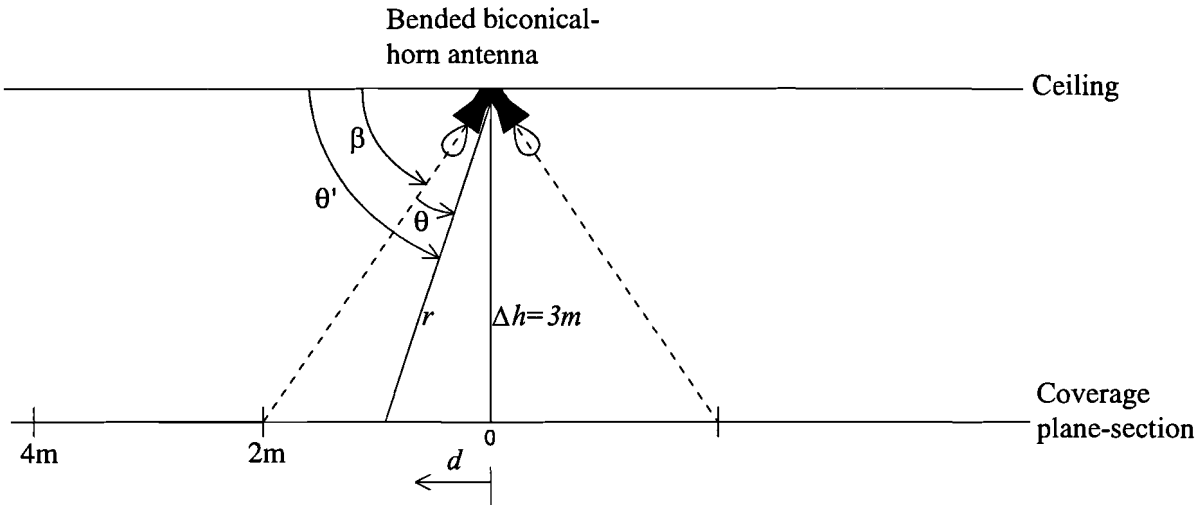


*Fig. 3.2: Geometry of the rays from the bended biconical-horn antenna*

In Fig. 3.2, the variable *d* gives the distance from the central point of the coverage plane-section. It varies from 0 to 4 metre.

To determine the required coverage of the bended biconical horn-antenna, '$\beta$' must be introduced into the formulas. For this it is obvious that $\cos\theta$ in equation (2.1) and $\sin\theta$ in equation (2.2) are replaced by expression (3.1) and (3.2), respectively.

$$\cos\theta = \frac{\Delta h}{r}\,\frac{1}{\cos\beta\,\tan\left[\arcsin\left(\frac{\Delta h}{r}\right)-\beta\right]+\sin\beta} \tag{3.1}$$

$$\sin\theta = \frac{\Delta h}{r}\,\frac{\tan\left[\arcsin\left(\frac{\Delta h}{r}\right)-\beta\right]}{\cos\beta\,\tan\left[\arcsin\left(\frac{\Delta h}{r}\right)-\beta\right]+\sin\beta} \tag{3.2}$$

A derivation of expression (3.1) and (3.2) is given in Appendix A. Now for the boundaries of the Fresnel integrals for the bended biconical-horn antenna, expression (3.3) and (3.4) are valid.

$$r_1 = 2\sqrt{s}\left[-1-\frac{1}{4s}\left(\frac{A}{\lambda}\frac{\Delta h}{r}\frac{\tan\left[\arcsin\left(\frac{\Delta h}{r}\right)-\beta\right]}{\cos\beta\,\tan\left[\arcsin\left(\frac{\Delta h}{r}\right)-\beta\right]+\sin\beta}\right)\right] \tag{3.3}$$

$$r_2 = 2\sqrt{s}\left[1-\frac{1}{4s}\left(\frac{A}{\lambda}\frac{\Delta h}{r}\frac{\tan\left[\arcsin\left(\frac{\Delta h}{r}\right)-\beta\right]}{\cos\beta\,\tan\left[\arcsin\left(\frac{\Delta h}{r}\right)-\beta\right]+\sin\beta}\right)\right] \tag{3.4}$$

Then, the structure function $F(\theta,s)$ is equal to

$$\left|F(\theta',s)\right| = \frac{\left|E(\theta')\right|}{\left|E(0)\right|} = \frac{1+\cos\theta}{2}\left[\frac{\left[C(r_2)-C(r_1)\right]^2+\left[S(r_2)-S(r_1)\right]^2}{4\left[C^2\left(2\sqrt{s}\right)+S^2\left(2\sqrt{s}\right)\right]}\right]^{1/2}. \tag{3.5}$$

where $\cos\theta$ is replaced by the expression given in equation (3.1).

The parameter $s$ is the same as in (2.4)

$$s = \frac{1}{8}\left(\frac{A}{\lambda}\right)^2\frac{1}{1/\lambda}\ . \tag{3.6}$$

The directivity is now equal to

$$D(\theta',s) = \frac{4\pi}{\int_0^{2\pi}\int_{-\pi/2}^{\pi/2}\left|F(\theta')\right|^2\cos\theta'\,d\theta'\,d\varphi}\ . \tag{3.7}$$

The power received by the MPS (isotropic) antenna is equal to

$$P_r(r,\theta',s) \propto D(\theta',s)\left|F(\theta')\right|^2\left[\frac{\lambda}{4\pi r}\right]^2. \tag{3.8}$$

This formula for the calculation of the received power, can be expressed as a function of the horizontal distance $d$ as it is shown in Fig. 3.3.

$$P_r(d,\beta,s) \propto D(\theta',s)\left|F(\theta')\right|^2\left[\frac{\lambda}{4\pi\sqrt{d^2+(\Delta h)^2}}\right]^2 \tag{3.9}$$

By taking a suitable value for the ratio $A/\lambda$, the optimum coverage of the bended biconical-horn antenna can be determined. In Fig. 3.3, the coverages for various values of $s$ are shown. These cover-

ages show the by the isotropic MPS-antennas received power relative to the maximum power against the horizontal distance $d$. This has been done for some values of β with the parameters: $\lambda$ = 5 mm, $\Delta h$ = 3 m and $A/\lambda$ =6 [1]. The curves are normalized to the maximum value for s= 0.5. The value of $A/\lambda$ has been taken the same as for the untilted biconical-horn antenna. If the beams of the 2 horns overlap each other, then the formulas described before are not valid anymore. So, the value of β must be limited to a maximum. The angle of bending β has been determined by taking equidistant radii $d$ of circles on the coverage plane-section (see Fig. 3.2). The angle of bending β can be calculated by

$$\beta = 90 - \arctan\left(\frac{d}{\Delta h}\right). \tag{3.10}$$

In table 3.1, the values of $d$ and β are given.

| $d$ [m] | β [degrees] |
|---|---|
| 1 | 71 |
| 2 | 56 |
| 3 | 45 |

Table 3.1: Angle of bending

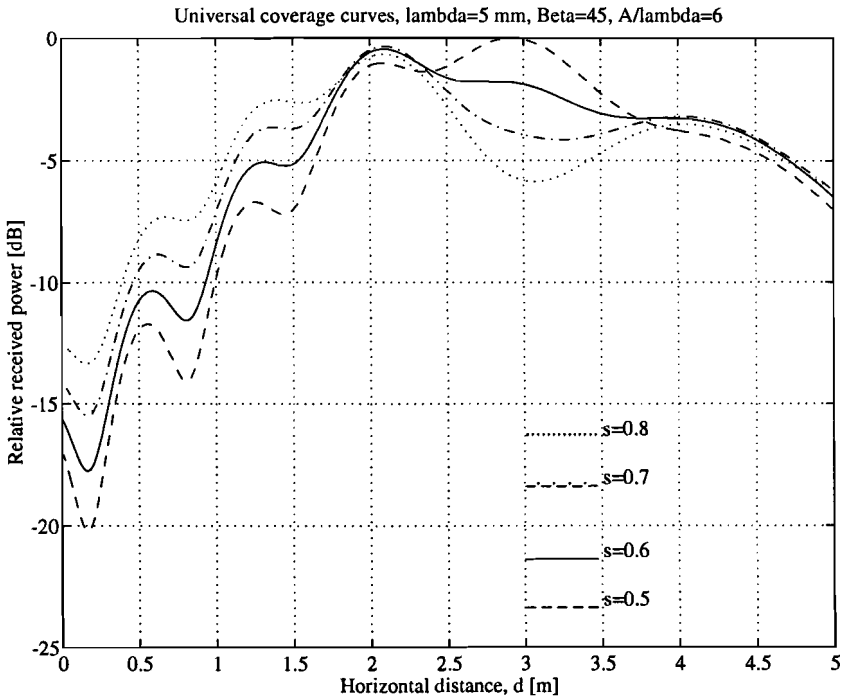


*Fig. 3.3a: Universal coverage curves for β=45° with s as parameter*

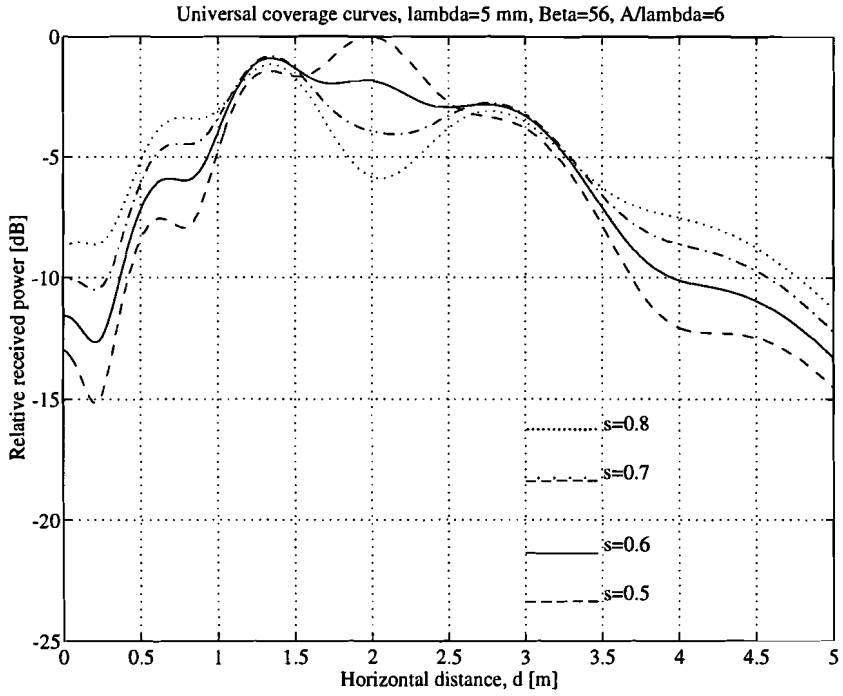


*Fig. 3.3b: Universal coverage curves for β=56° with s as parameter*

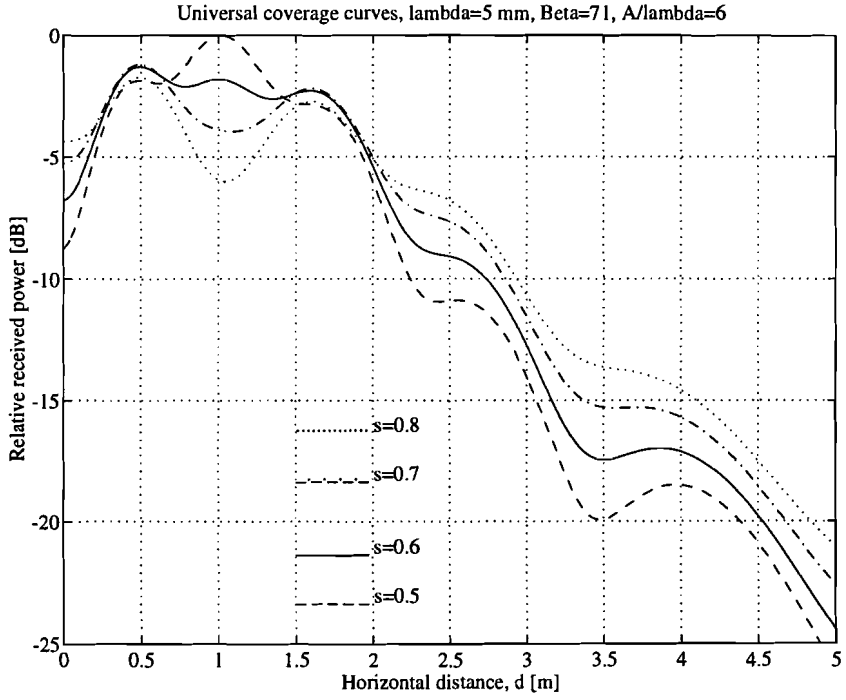


*Fig. 3.3c: Universal coverage curves for β=71° with s as parameter*

From all these universal coverage curves we can see that the coverage in the area from $d$ = 0 to $d$ = 4 m is not constant. For $\beta = 56°$ (see Fig.3.3 b), we can see that the coverages are fluctuating. If we take for instance the coverage with $s$ = 0.6 ($\beta = 56°$), we can observe that it fluctuates within 3 dB in the area between $d$ = 1 to $d \approx 3.2$ m. From $d$ = 0 to $d$ =1 m and from $d \approx 3.2$ to $d$ =5 m, it decreases quickly. Hence, we can conclude that there is a ring-shaped coverage area with a ring width of about 2 m. If $\beta$ is increasing, then the ring-shaped coverage area becomes narrower and it slides to the centre. A sketch of the footprint of the ring-shaped coverage area is depicted in Fig.3.4.

The coverage for $\beta = 71°$ (Fig. 3.3c) is an example where we can see that the beams of the 2 horns are just overlapping. So, we can conclude that the maximum angle of bending $\beta = 71°$.

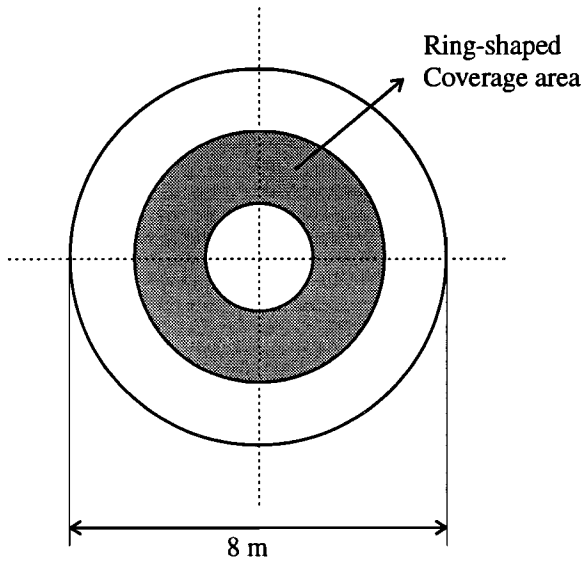


*Fig. 3.4: Footprint of the bended biconical-horn antenna*

In Fig.3.5, coverages are shown for various values of $A/\lambda$ at $\beta = 56°$ where $s$=0.6, $\lambda$ = 5 mm and $\Delta h$ = 3 m. In this figure, we can see that as the term $A/\lambda$ decreases, the ring-shaped coverage area becomes wider, but on the other hand the fluctuation in the ring-area becomes higher.

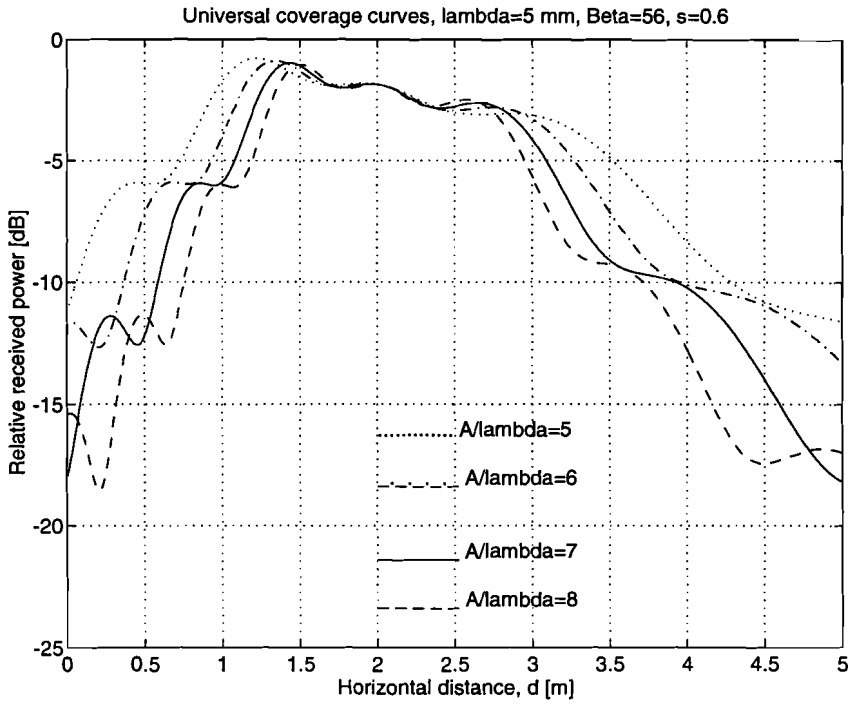


*Fig. 3.5: Universal coverage for* $\beta$*=56° and s=0.6 with A/*$\lambda$ *as parameter*

The conclusions that we can take from these computations are:

- $\beta$ establishes the ring-coverage on the coverage plane-section
- the uniformity of the ring-coverage can be arranged with $s$
- the width of the ring-area can be arranged with $A/\lambda$

Now, from these computations we can determine the optimum values of $\beta$, $s$ and $A/\lambda$. These are:

- $45° \leq \beta \leq 71°$
- $s = 0.6$
- $A/\lambda = 6$

# 4. The reflector antenna

## 4.1 General approach

As is mentioned in the general introduction, the reflector antenna is the second option that will be investigated for indoor radio communication system. The design of this antenna is based on the theory of a shaped double reflector antenna as is shown in Fig. 4.1 [4].

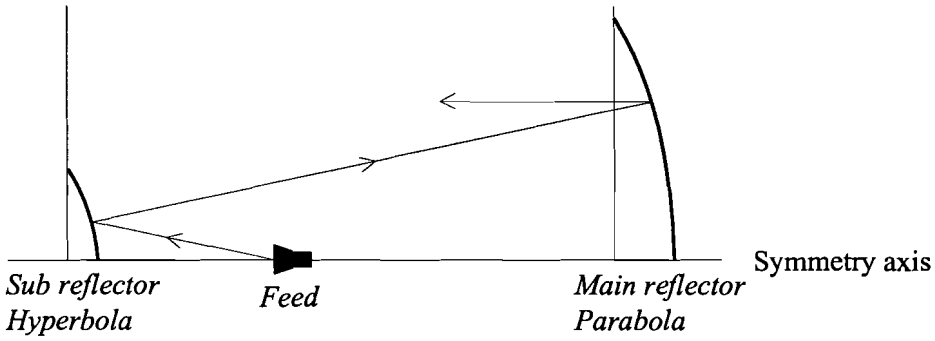


*Fig. 4.1: Double reflector antenna*

In this design the feed is a conical corrugated-horn antenna that has a radiation pattern $G_f(\psi)$ with the form of a cosine to the power n. The main reflector of the original double reflector antenna is replaced by the coverage plane-section. That means that this is a single reflector antenna system (see Fig. 4.2). The antenna is fixed to the ceiling (3 metres above the coverage plane-section).

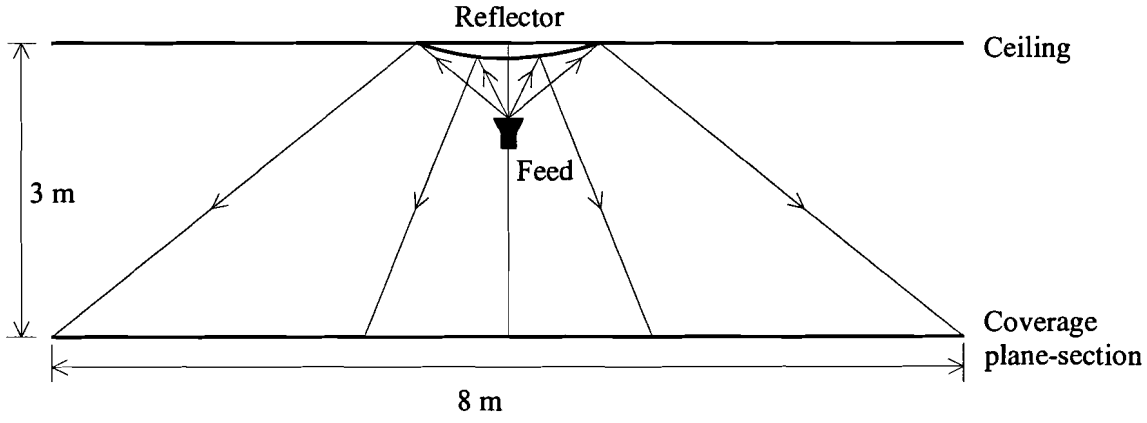


*Fig. 4.2: The reflector antenna in the MEDIAN demonstrator scenario*

The objectives of this thesis is to examine the relationship between the surface shape of the reflector and the variation of the field (ripple) over the coverage plane-section. Furthermore, we have to determine a surface of acceptable dimensions in the order of (20-30 cm) that yields an acceptable ripple (e.g. 1 dB). There are some assumptions on the design of this antenna system, these are:

- The reflector is placed on a height of three metre from the coverage plane-section.
- The field is constant within the coverage plane-section that has a diameter of 8 metre.

Because the carrier frequency is very high ($f = 60$ GHz, $\lambda = 5$ mm), we use geometrical optics for the design of the reflector antenna. Because of the use of geometrical optics, the design of the reflector antenna must satisfy the following conditions:

1. The law of *Snel* for reflecting surface: angle of incidence is equal to angle of reflection with respect to the normal vector.
2. Law of conservation of power: the energy per unit of time that passes through a surface within a ray tube is independent of that surface (see Fig. 4.3). The energy in the circle surface on the reflector is equal to the energy in the circle surface on the coverage plane-section. So the powerflow in a ray tube is constant.
3. The law of *Malus*: the surfaces of constant phase are surfaces perpendicular to the rays, also after one or more reflections.

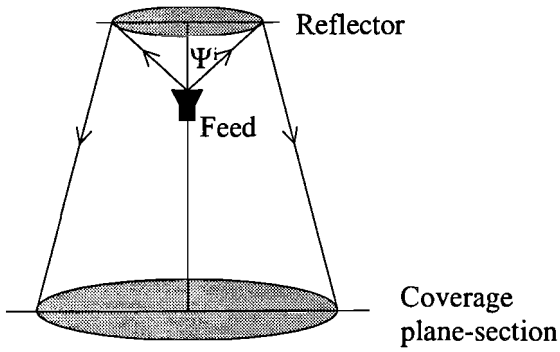


*Fig. 4.3: Power conservation*

Applying these conditions on the antenna system leads to a number of equations which the system must satisfy. Application of Snel's law of reflection for the reflector (see Fig. 4.4) leads to the following differential equation

$$\frac{dy_r}{dx_r} = \tan\left[\tfrac{1}{2}\Psi^i - \tfrac{1}{2}\Psi^r\right], \tag{4.1}$$

where $\Psi^i$ and $\Psi^r$ are the angle of incidence and angle of reflection, respectively, with respect to the horizontal plane.

$$\tan(\Psi^i) = \frac{x_r}{F - y_r} \quad \Leftrightarrow \quad \Psi^i = \arctan\left(\frac{x_r}{F - y_r}\right), \tag{4.2}$$

$$\tan(\Psi^r) = \frac{x_c - x_r}{3 - y_r} \quad \Leftrightarrow \quad \Psi^r = \arctan\left(\frac{x_c - x_r}{3 - y_r}\right). \tag{4.3}$$

Substitution of (4.2) and (4.3) into (4.1) yields the following differential equation

$$\frac{dy_r}{dx_r} = \tan\left[\tfrac{1}{2}\arctan\left(\frac{x_r}{F - y_r}\right) - \tfrac{1}{2}\arctan\left(\frac{x_c - x_r}{3 - y_r}\right)\right]. \tag{4.4}$$

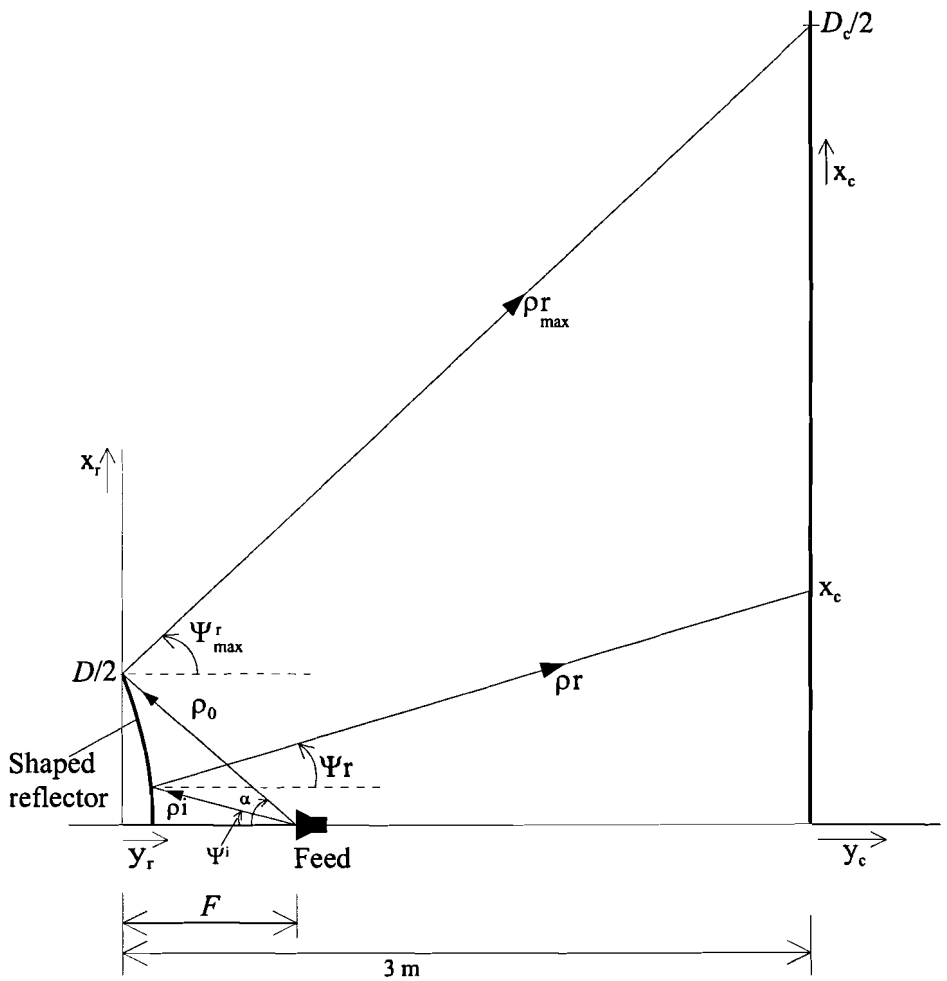


*Fig. 4.4: Geometry of the rays of the shaped reflector antenna*

There are two coordinate systems in Fig. 4.4, one describes the coordinates $(x_r,y_r)$ of the reflector and the other one describes the coordinates $(x_c,y_c)$ of the coverage plane-section. The parameters used in this figure are described below. Because of the rotationally symmetry with respect to the horizontal axis of the antenna system, only the situation for $x_r>0$ is described.

$(x_r,y_r)$ a coordinate point of the reflector

$(x_c,y_c)$ a coordinate point of the coverage plane-section

$\rho^i$ the ray length from the feed to the reflector

$\rho_0$ the maximum ray length from the feed to the reflector

$\rho^r$ the length of the reflected ray

$\rho^r_{max}$ the maximum length of the reflected ray

$\Psi^i$ the angle between the horizontal axis and the ray from the feed

$\alpha$ the maximum angle between the horizontal axis and the ray from the feed

$\Psi^r$ the angle between the horizontal axis and the reflected ray

$\Psi^r_{max}$ the maximum angle between the horizontal axis and the reflected ray

$D$ diameter of the reflector

$D_c$ diameter of the coverage plane-section

$F$ the distance between the feed and the origin of $(x_r,y_r)$ coordinate system

Because of the rotational symmetry of the antenna system, the relative power radiated by the feed between the angles 0 and $\Psi^i$ can be written as

$$P_f = 2\pi \int_0^{\Psi^i} G_f(\psi)\, \sin\psi \, d\psi \ , \tag{4.5}$$

with $G_f(\Psi)$ the gain function of the feed

$$G_f(\Psi) = \begin{cases} 2(n+1)\cos^n(\Psi) & \text{for} \quad 0 \le \Psi \le \frac{\pi}{2} \\ 0 & \text{for} \quad \Psi > \frac{\pi}{2} \end{cases} \ . \tag{4.6}$$

According to the second condition, the relative power given in equation (4.5) is equal to

$$P_f = 2\pi \int_0^{x_c} H(r)\, r\, dr \ , \tag{4.7a}$$

with $H(r)$ the illumination function of the coverage plane-section. The reflected powerflux $\vec{S}$ flows not perpendicularly through the coverage plane-section. So, it must be corrected by taking the in-product of the power flux and the normal vector to the coverage plane (see Fig. 4.5).

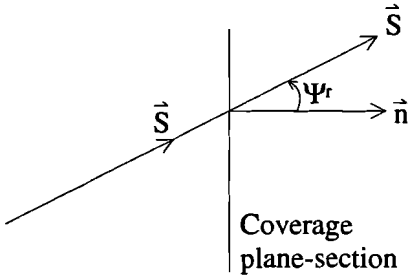


*Fig. 4.5: Power flux through the coverage plane-section*

The absolute value of the powerflux flowing perpendicularly through a surface is equal to $|\vec{S}| = \frac{|\vec{E}|^2}{2Z_0}$, with $\vec{E}$ the electric field and $Z_0$ the intrinsic impedance of free space. Generally, the powerflux flowing through a surface is equal to $|\vec{S}| = \frac{|\vec{E}|^2}{2Z_0}\cos\Psi^r$. Since the illumination function $H(r) \propto |\vec{S}|$, the power intercepted by a circle with radius '$x_c$' on the coverage plane-section is equal to

$$P_f = 2\pi \int_0^{x_c} H(r)\cos(\Psi^r)\, r\, dr \tag{4.7b}$$

After normalizing equation (4.5) and (4.7b) to the total radiated power by the feed to the reflector and then combining these equations, yields

$$\frac{\int_0^{x_c} H(r)\cos(\Psi^r(r))\, r\, dr}{\int_0^{D_c/2} H(r)\cos(\Psi^r(r))\, r\, dr} = \frac{\int_0^{\Psi^i} G_f(\psi)\sin\psi\, d\psi}{\int_0^{\alpha} G_f(\psi)\sin\psi\, d\psi} \tag{4.8}$$

Here $D_c = 8$ m.

Furthermore, there are two boundary conditions, these are:

$$\tan\alpha = \frac{D}{2F}, \tag{4.9}$$

and

$$\tan(\Psi^r_{max}) = \frac{D_c - D}{6}. \tag{4.10}$$

Now with $\Psi^i$, $\Psi^r$, the ratio $D/D_c$, $H(r)$, $G_f(\Psi^i)$, the total system is determined. If for instance $x_c$ is given, then $x_r$, $y_r$ and further $\Psi^i$, $\Psi^r$ can be calculated.

# 4.2 *Design of shaped reflector antenna*

To determine the shape of the reflector surface, the coordinates $(x_r,y_r)$ must be calculated. The essence of the design of the reflector is that the field in the coverage plane-section has an acceptable ripple. Outside the coverage plane-section the field must be as low as possible. The spatial fluctuation of the field on the coverage plane must be below a specified limit. Hence, the illumination function $H(r)$ of the coverage plane should be constant and equation (4.8) can be simplified to

$$\frac{\int_0^{x_c} \cos(\Psi^r(r))\, r\, dr}{\int_0^{D_c/2} \cos(\Psi^r(r))\, r\, dr} = \frac{\int_0^{\Psi^i} G_f(\psi)\sin\psi\, d\psi}{\int_0^{\alpha} G_f(\psi)\sin\psi\, d\psi} \quad . \tag{4.11}$$

Substitution of equation (4.3) and (4.6) in equation (4.11) yields

$$\frac{\int_0^{x_c} \cos\left[\arctan\left(\frac{r-x_r}{3-y_r}\right)\right] r\, dr}{\int_0^{D_c/2} \cos\left[\arctan\left(\frac{r-x_r}{3-y_r}\right)\right] r\, dr} = \frac{\int_0^{\Psi^i} 2(n+1)\cos^n\psi \sin\psi\, d\psi}{\int_0^{\alpha} 2(n+1)\cos^n\psi \sin\psi\, d\psi} \quad . \tag{4.12}$$

The solution of the left integrals of (4.12) have an analytical expression calculated by the mathematical software 'Mathematica' [15]. The solution of the numerator is equal to

$$\int_0^{x_c} \cos\left[\arctan\left(\frac{r-x_r}{3-y_r}\right)\right] r\, dr = -(y_r-3)\left[x_r \operatorname{arcsinh}\left(\frac{x_c-x_r}{y_r-3}\right) + x_r \operatorname{arcsinh}\left(\frac{x_r}{y_r-3}\right) + \right.$$
$$\left. + |y_r-3| \cdot \sqrt{9+x_r^2-2x_r x_c+x_c^2-6y_r+y_r^2} - \sqrt{9+x_r^2-6y_r+y_r^2}\right] \quad . \tag{4.13}$$

The solution of the denominator is equal to

$$\int_0^{D_c/2} \cos\left[\arctan\left(\frac{r-x_r}{3-y_r}\right)\right] r\, dr = -(y_r-3)\left[x_r \operatorname{arcsinh}\left(\frac{D_c/2-x_r}{y_r-3}\right) + x_r \operatorname{arcsinh}\left(\frac{x_r}{y_r-3}\right) + \right.$$
$$\left. + |y_r-3| \cdot \sqrt{9+x_r^2-2x_r D_c/2+(D_c/2)^2-6y_r+y_r^2} - \sqrt{9+x_r^2-6y_r+y_r^2}\right] \quad . \tag{4.14}$$

The solution of right integrals of (4.12) gives also an analytical expression.

$$\frac{\int_0^{\Psi^i} 2(n+1)\cos^n\psi \ \sin\psi \, d\psi}{\int_0^{\alpha} 2(n+1)\cos^n\psi \ \sin\psi \, d\psi} = \frac{\cos^{n+1}(\Psi^i)-1}{\cos^{n+1}\alpha - 1} \quad . \tag{4.15}$$

Combining (4.12) with (4.15) and using (4.2) for $\Psi^i$ and the boundary condition (4.9) for $\alpha$ yields the power equation

$$\frac{\int_0^{xc} \cos\left[\arctan\left(\frac{r-x_r}{3-y_r}\right)\right] r\,dr}{\int_0^{D_c/2} \cos\left[\arctan\left(\frac{r-x_r}{3-y_r}\right)\right] r\,dr} = \frac{\cos^{n+1}\left[\arctan\left(\frac{x_r}{f-y_r}\right)\right]-1}{\cos^{n+1}\left[\arctan\left(\frac{D}{2f}\right)\right]-1} \quad , \tag{4.16}$$

where the numerator and the denominator of the left part must be replaced by the expressions (4.13) and (4.14), respectively.

To calculate the surface function of the reflector, the differential equation given in (4.4) has to be solved numerically for a given value of $x_c$. By using a Pascal Procedure for the solution of the differential equation, a lot of pairs of $(x_r,y_r)$ coordinates are produced. These $(x_r,y_r)$ coordinates must be substituted into the power equation (4.16). If a single pair of $(x_r,y_r)$ coordinates satisfy the power equation, then that pair of coordinates is a unique point of the reflector that is valid for the given $x_c$ value. Before substituting the $(x_r,y_r)$ coordinates into the power equation, the value of $n$ in (4.16) has to be known. The value of $n$ is related to the illumination from the feed.

Determination of $n$:

Assume that the ray power from the feed to edge of the reflector is -10 dB compared with the ray to the centre of the reflector and the semiflare angle of the feed '$\alpha$' is equal to 45° (see Fig.4.6).

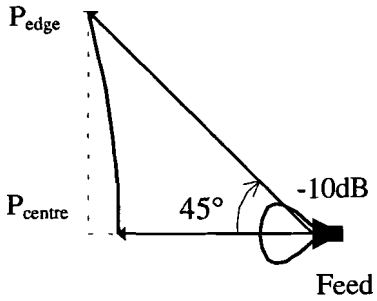


*Fig. 4.6: Edge Illumination from the feed*

$G_f = 2(n+1)\cos^n(\Psi)$

$\alpha = 45°$

$P_{edge} = 2(n+1)\cos^n(45)$

$P_{centre} = 2(n+1)\cos^n(0)$

Edge illumination from the feed = -10 dB

$P_{edge} = 0.1\ P_{centre}$

$2(n+1)\cos^n(45°) = 0.1\ \ 2(n+1)\cos^n(0)$

$\ln[\cos^n(45°)] = \ln[0.1]$

$$n = \frac{\ln[0.1]}{\ln[\cos(45)]} = 6.6$$

There are some values of $n$ given in Table 4.1 for different edge illuminations from the feed to reflector edge and $\alpha = 45°$.

| | $\alpha = 45°$ | | |
|---|---|---|---|
| edge illumination from the feed (dB) | -10 | -20 | -30 |
| $n \approx$ | 7 | 13 | 20 |

*Table 4.1: Values of n for different edge illuminations from the feed*

For the determination of the edge illuminations at the reflector, the free space loss from the feed to the reflector edge must be taken into account.

There is another point that deserves attention. During the substitution of the $(x_r,y_r)$ coordinates in the power equation, we saw at first that there weren't any $(x_c,y_c)$ points that satisfied the power equation. The reason of this is that the values of $x_c$ along the coverage plane are equidistant values. The values of $x_r$ along the reflector are also (lower) equidistant values. To solve this problem we have introduced a relative error '$\varepsilon_{rel}$' in equation (4.16) and we got another power equation given in (4.17). The physical meaning of '$\varepsilon_{rel}$' is that the power radiated by the feed is not anymore equal to the power on the coverage plane-section but it slightly deviates from it.

$$\underbrace{\frac{\int_0^{x_c} \cos\left[\arctan\left(\frac{r-x_r}{3-y_r}\right)\right] r\,dr}{\int_0^{D_c/2} \cos\left[\arctan\left(\frac{r-x_r}{3-y_r}\right)\right] r\,dr}}_{p_1} = \underbrace{\frac{\cos^{n+1}\left[\arctan\left(\frac{x_r}{f-y_r}\right)\right]-1}{\cos^{n+1}\left[\arctan\left(\frac{D}{2f}\right)\right]-1}}_{p_2} + \varepsilon_{rel}\ . \qquad (4.17)$$

with

$p_1$: Relative power on the coverage plane-section,

$p_2$: Relative power radiated by the feed.

The relative error '$\varepsilon_{rel}$' is defined as

$$\varepsilon_{rel} = \left| \frac{p_1 - p_2}{p_2} \right| . \tag{4.18}$$

Expression (4.18) can be written as

$$\left| \frac{p_1}{p_2} \right| = (1 \pm \varepsilon_{rel}) \tag{4.19a}$$

and in (dB)

$$10 \log \left| \frac{p_1}{p_2} \right| = 10 \log (1 \pm \varepsilon_{rel}) . \tag{4.19b}$$

The power difference on the coverage plane-section related to the power radiated by the feed can be calculated by equation (4.19). Hence, the electric field can also be calculated. This is given in Table 4.2 for different values of '$\varepsilon_{rel}$'.

| Power and E-field on the coverage plane-section | $\varepsilon_{rel}$ 1e-5 | 1e-4 | 1e-3 | 1e-2 |
|---|---|---|---|---|
| $P_{dB}$=10 log (1±$\varepsilon_{rel}$) | ±4.34 e-5 dB | ±4.34 e-4 dB | ±4.34 e-3 dB | ±4.32 e-2 dB |
| $E_{dB}$= 20 log$\sqrt{p}$ | ±4.34 e-5 dB | ±4.34 e-4 dB | ±4.34 e-3 dB | ±4.32 e-2 dB |
| $E_{\%\ ripple}$ | 0.005 % | 0.005 % | 0.05 % | 0.5 % |

*Table 4.2: The effect of the relative error '$\varepsilon_{rel}$' to the field in the coverage plane-section*

# 4.3 *Example of shaped reflector antenna*

In this section, the shape of the reflector antenna is given. The design of the reflector is based on the theory described in the previous section. To determine the shape of the reflector surface, some assumptions are made and there are some boundary conditions.

Assumptions: $D_c$ = 8 m

$D$ = 30 cm

Edge ill. from feed = -10 dB

$F/D$ = 0.5

Boundary conditions: $x_r = 0$ for $x_c = 0$

$x_r = D/2$ and $y_r = 0$ for $x_c = 4$ m

Input parameter: $x_c$

Output variable: $x_r$, $y_r$

The reason why the edge illumination from the feed has been taken -10 dB is that the spillover and the blocking are acceptable. An edge illumination from the feed of -20 dB yields a lower spillover, but the blocking becomes higher.

The value of $x_c$ varies from zero to 4 m with a step size of 1 cm. For every value of $x_c$, there is one $(x_r,y_r)$ calculated coordinate pair that satisfies the power equation.

The relative error '$\varepsilon_{rel}$' varies from (9 e-7) to (1 e-2). The variations of the power on the coverage plane-section related to the power from the feed are given below.

$P_{dB}$= (3.9 e-6 --------- 4.32 e-2) dB

and

$E_{\%\ ripple}$ = (9 e-5 --------- 0.50) %

So, we can see that the fluctuation in this case is negligible small.

A cross-section of the entire shaped reflector with $F/D$=0.5 is depicted in Fig. 4.7. In Fig. 4.7, the cross-sections of the shaped reflectors for $F/D$=0.4; $F/D$=0.6; $F/D$=0.7 are also drawn to observe the effect of shaping of the reflector when the $F/D$-ratio changes. The reflector diameter of 30 cm and the edge illumination at the feed of -10 dB have been taken fixed for all these reflectors. From Fig. 4.7 we can see that the depth of the reflector is increasing as the $F/D$-ratio increases.

The ray pattern of the antenna with $F/D$=0.5 is drawn in Fig 4.8. In this figure, the angle between the rays from the feed is about 2°. Between the incident and reflected rays, the law of **Snel** is satisfied.

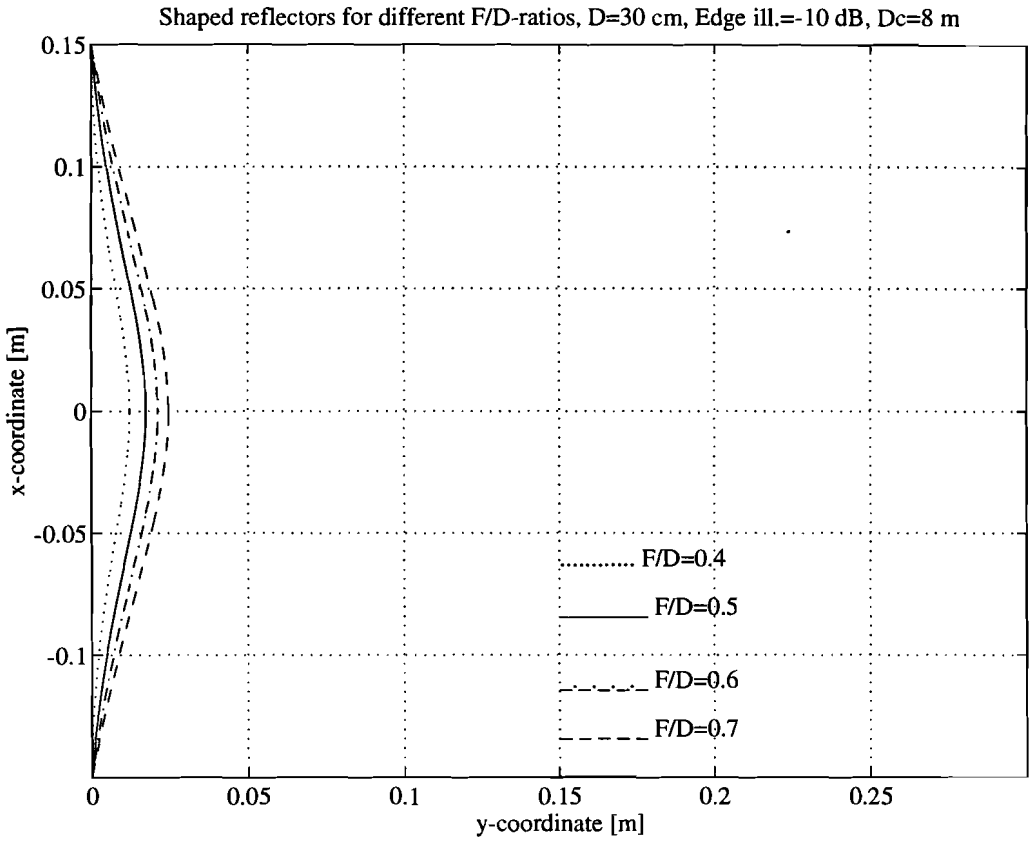


*Fig. 4.7: The shaped reflector antennas for different F/D-ratios*

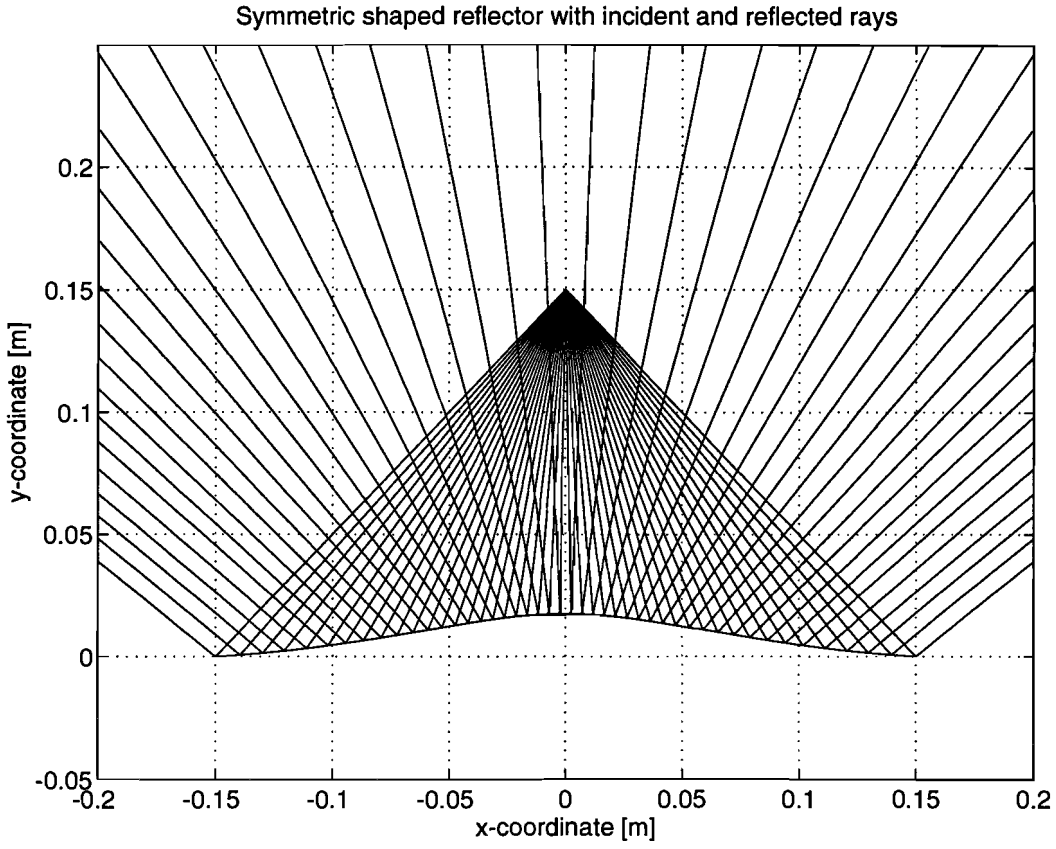


*Fig. 4.8: Ray pattern of the shaped reflector antenna for F/D=0.5*

Ray pattern of shaped reflector antenna with the following specifications:

- Diameter reflector $D$ = 30 cm
- $F/D$ = 0.5
- Edge illumination at feed = -10 dB
- Diameter of coverage plane-section $D_c$ = 8 m
- Angle between the rays from feed = 2°

In the next chapter, the calculation of the diffracted field using UTD and the total field on the coverage plane-section are described.

# 5. UTD Analysis of the radiation from the shaped reflector antenna

## 5.1 Introduction

The GTD (Geometrical Theory of Diffraction) ([9],[11],[12]) describes the diffraction phenomena by introducing various kinds of diffracted rays, such as single-diffracted rays and multiple-diffracted rays. The corresponding diffracted waves are assumed to follow the laws of diffraction and to diverge according to GO laws. Consequently, the points of diffraction and the paths of the rays can be found from the laws of diffraction, and the amplitude of the fields along the rays can be found from the principle of energy conservation. So, this theory does not only provide a qualitative description of diffraction in terms of the diffracted rays, but also permits a quantitative determination of the diffracted field as well. In this report only single-diffracted rays are considered. So, the small contributions of multiple-diffracted rays are neglected.

The initial value of the diffracted field at the point of diffraction is obtained by multiplying the vector of the incident wave by the dyadic diffraction coefficient, which was first obtained by Keller by comparing his diffraction expressions with Sommerfeld's exact solutions for various canonical problems. Although the diffraction coefficients are derived for canonical problems, such as the diffraction of a plane, cylindrical, conical or spherical wave at perfectly conducting infinite half plane or wedge, the theory can be used to calculate the field diffracted from other objects as long as their dimensions are large compared to the wavelength. In that case only the immediate neighbourhood of points of diffraction effectively contributes so that the diffraction can be considered as a local phenomenon.

According to Keller's GTD ([11], [12]), the contributions to the field in an observation point $P(r,\theta,\phi)$ come, in the case of the symmetrical reflector antenna (see Fig. 5.1 ), mainly from two points Qi (i=1,2), which are the intersection points of the plane containing the lines O'P and O'F with the edge of the reflector. UTD (Uniform Geometrical Theory of Diffraction) gives diffraction coefficients which are also valid in the shadow and reflection boundary where Keller's theory fails. UTD gives a compact form of the dyadic diffraction coefficient for electromagnetic waves obliquely incident on a curved edge (of a perfectly conducting reflector surface). Since UTD is basically an extension of GTD, they both are based on the same principles.

The coordinates of the diffraction points are given by (Fig. 5.1) [7]:

$$\xi_1 = \phi \tag{5.1a}$$

$$\xi_2 = \phi + \pi \tag{5.1b}$$

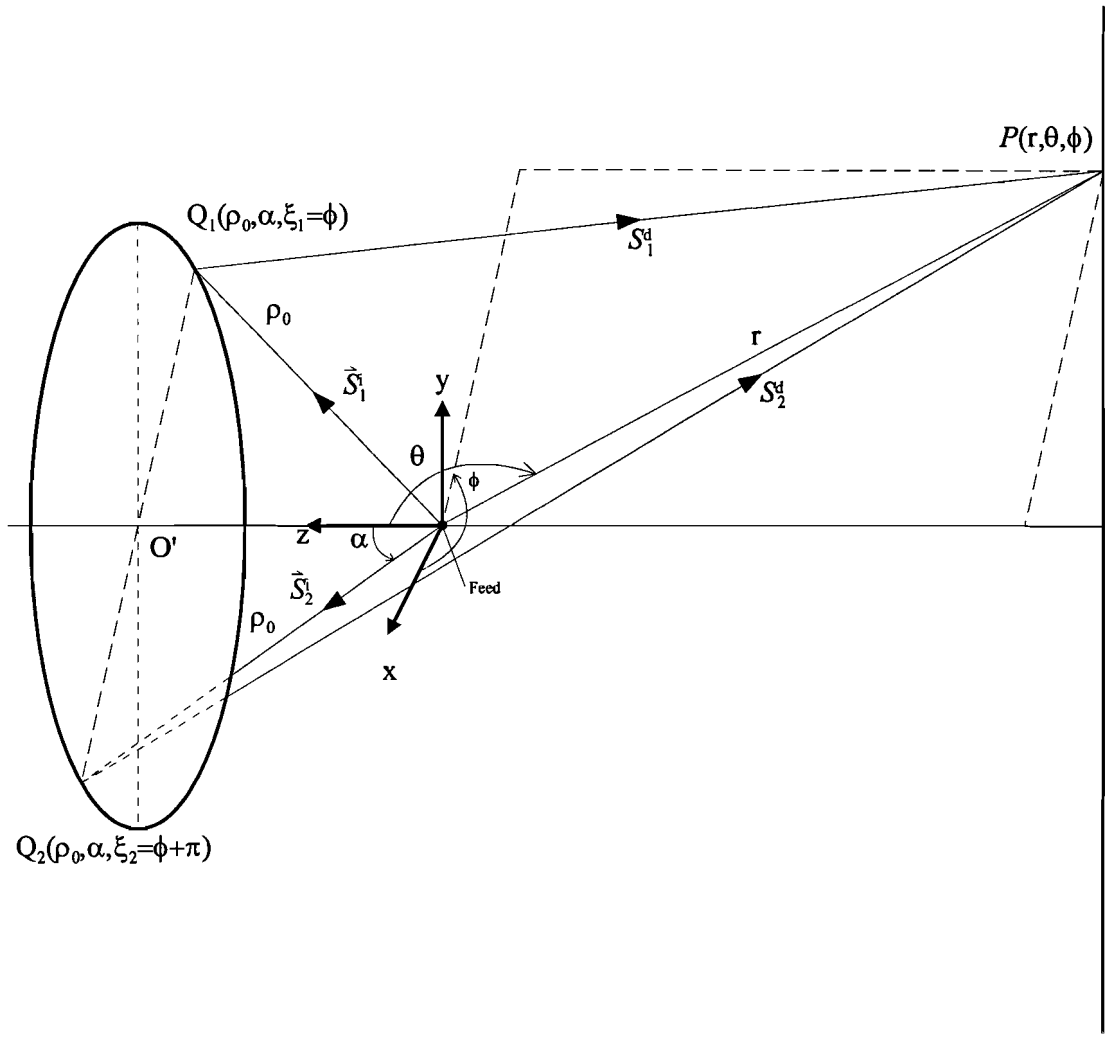


*Fig. 5.1: Geometry of diffracted rays*

The diffracted field $E^d(P)$ due to the diffraction point $Q_i$ can be expressed by [10]:

$$\vec{E}^d(p) = \vec{D} \cdot \vec{E}^i(Q_i)\ A(s_i^i, s_i^d)\ e^{-jks_i^d} \tag{5.2}$$

where $\vec{D}$ the is the dyadic diffraction coefficient, $A(s_i^i, s_i^d)$ is the caustic divergence factor, $s_i^i$ is the distance from the feed to the point of diffraction, $s_i^d$ is the distance from the point of diffraction to the observation point and $\vec{E}^i(Q_i)$ is the incident field at point $Q_i$. Because $Q_1$, $Q_2$, P, F and O' are lying in the same $\phi$ -plane, we can consider the case as a two dimensional problem and only take a single $\phi$ -plane to analyze the diffracted fields as shown in Fig. 5.2.

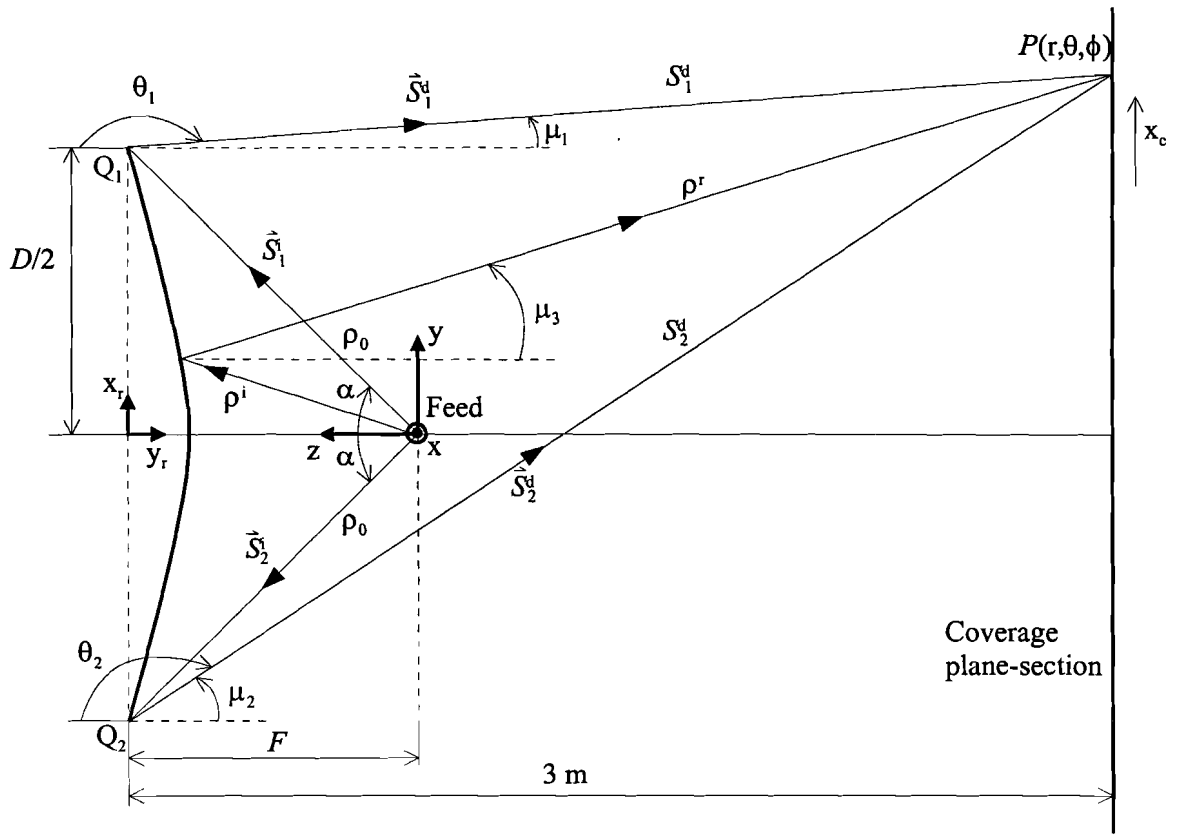


*Fig. 5.2: Two dimensional geometry to analyze the diffraction field*

The distances given in Fig. 5.2 are described below:

$$\rho_0 = \sqrt{\left(\frac{D}{2}\right)^2 + F^2} \tag{5.3}$$

$$\rho^i = \sqrt{x_r^2 + (F - y_r)^2} \tag{5.4}$$

$$\rho^r = \sqrt{(x_c - x_r)^2 + (3 - y_r)^2} \tag{5.5}$$

$$s_1^d = \sqrt{\left(x_c - \frac{D}{2}\right)^2 + 9} \tag{5.6}$$

$$s_2^d = \sqrt{\left(x_c + \frac{D}{2}\right)^2 + 9} \tag{5.7}$$

$s_1^d$ and $s_2^d$ are the distances from the upper and lower edge of the reflector, respectively, to the observation point on the coverage plane-section.

To be able to calculate the diffracted field, the following procedure is followed. First the caustic divergence factor is determined followed by a derivation of the dyadic diffraction coefficients. This will be done in the following paragraphs.

## 5.2 *Calculation of Caustic Divergence factor*

For diffraction of an incident spherical wave at a curved edge, the caustic divergence factor takes the form [10] of equation (5.8). This is the general formula for the caustic divergence factor.

$$A_i(\rho_c, s_i^d) = \frac{1}{s_i^d}\sqrt{\frac{\rho_c\, s_i^d}{\rho_c + s_i^d}}\ , \tag{5.8}$$

where

$$\frac{1}{\rho_c} = \frac{1}{\rho_e^i} - \frac{\vec{n}\cdot(\vec{s}_i^{\,i} - \vec{s}_i^{\,d})}{\rho_g \sin^2\beta_0}\ . \tag{5.9}$$

The terms used in equation (5.9) represent the following:

$\rho_c$ the distance between the caustic at the edge and the second caustic of the diffracted ray,

$\rho_g$ the radius of the curvature of the edge at the diffraction point,

$\rho_e^i$ the radius of curvature of the incident wavefront at the edge, fixed plane of incidence which contains the unit vectors $\vec{s}_i^{\,i}$ and the unit vector $\vec{T}$ tangent to the edge at $Q_i$,

$\beta_0$ the angle between $\vec{s}_i^{\,i}$ and the tangent $\vec{T}$ to the edge at the point of diffraction,

$\vec{n}$ the unit vector normal to the edge at $Q_i$ and directed away from the centre of the curvature,

$\vec{s}_i^{\,i}$ the unit vector in the direction of the incident ray (Fig. 5.2),

$\vec{s}_i^{\,d}$ the unit vector in the direction of the diffracted ray (Fig 5.2).

In the following sections, equation (5.8) will be worked out for our specific geometry.

## 5.2.1 *Caustic divergence factor for the upper diffraction point $Q_1$*

In Fig. 5.3, the upper diffraction point $Q_1$ and the associated vectors are given in detail.

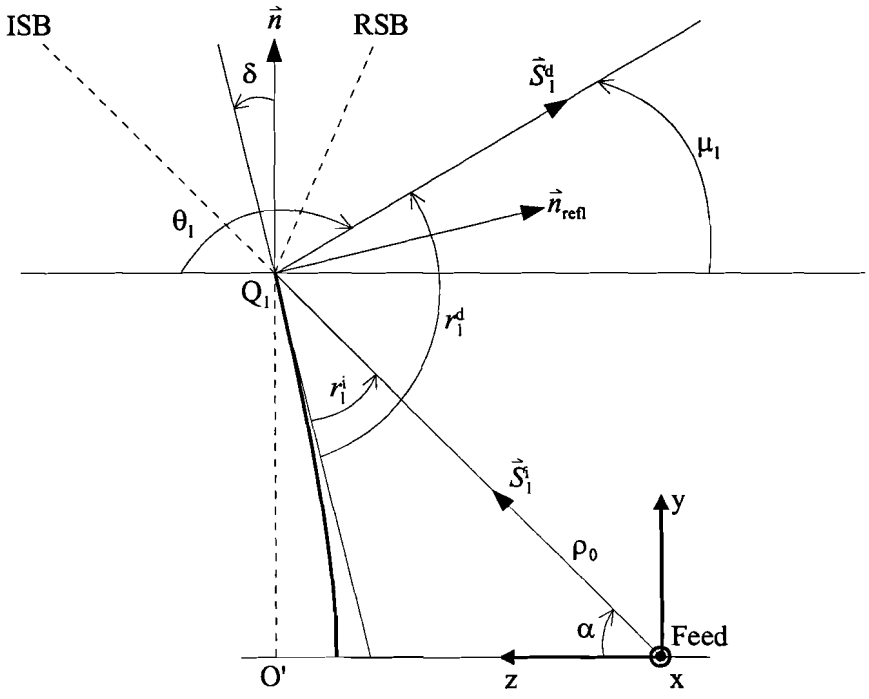


*Fig. 5.3: Geometry of incident and diffracted rays at $Q_1$*

From Fig. 5.2 and Fig.5.3 it is easy to find:

$$\vec{n} \cdot \vec{s}_1^{\,i} = \sin\alpha \ , \tag{5.10a}$$

$$\vec{n} \cdot \vec{s}_1^{\,d} = \sin\theta_1 \ , \tag{5.10b}$$

with

$$\alpha = \arctan\left(\frac{D}{2F}\right) \ , \tag{5.10c}$$

$$\theta_1 = \pi - \mu_1 \ , \tag{5.10d}$$

$$\mu_1 = \arctan\left(\frac{x_c - \frac{D}{2}}{3}\right) \ , \tag{5.10e}$$

$$\rho_e^i = \rho_0 \ , \tag{5.10f}$$

$$\rho_g = \frac{D}{2} \,, \tag{5.10g}$$

$$\beta_0 = \frac{\pi}{2} \,. \tag{5.10h}$$

Substituting equation (5.10) in equation (5.9), then Substituting the result of this into equation (5.8) gives the following expressions for $\rho_c$ and $A_1$, respectively:

$$\rho_{c1} = \rho_0 \frac{\sin\alpha}{\sin\theta_1} \,, \tag{5.11}$$

$$A_1\left(\rho_{c1}, s_1^d\right) = \frac{1}{s_1^d}\sqrt{\frac{s_1^d\ \rho_0 \sin\alpha}{\rho_0 \sin\alpha + s_1^d \sin\theta_1}} \,. \tag{5.12}$$

## 5.2.2 *Caustic divergence factor for the lower diffraction point $Q_2$*

In Fig. 5.4, the lower diffraction point $Q_2$ and the associated vectors are given in detail. For the lower diffraction point the following expressions are valid:

$$\vec{n} \cdot \vec{s}_2^{\,i} = \sin\alpha \,, \tag{5.13a}$$

$$\vec{n} \cdot \vec{s}_2^{\,d} = -\sin\theta_2 \,, \tag{5.13b}$$

with

$$\theta_2 = \pi - \mu_2 \,, \tag{5.13c}$$

$$\mu_2 = \arctan\left(\frac{x_c + \frac{D}{2}}{3}\right) \,, \tag{5.13d}$$

$$\rho_e^i = \rho_0 \,, \tag{5.13e}$$

$$\rho_g = \frac{D}{2} \,, \tag{5.13f}$$

$$\beta_0 = \frac{\pi}{2} \,. \tag{5.13g}$$

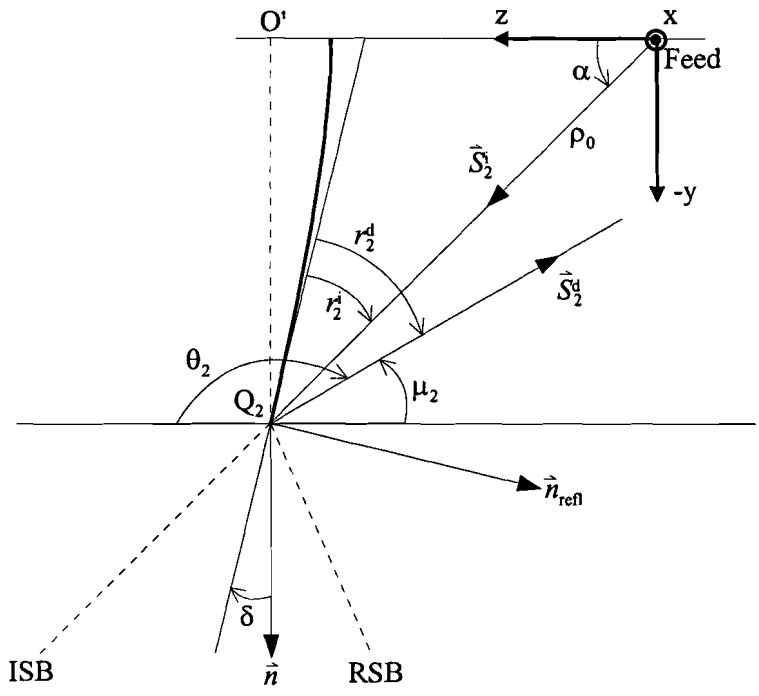


*Fig. 5.4: Geometry of incident and diffracted rays at $Q_2$*

Substituting equation (5.13) in equation (5.9) and then substituting the result into equation (5.8) gives the following expressions for $\rho_c$ and $A_1$, respectively:

$$\rho_{c2} = -\rho_0 \frac{\sin\alpha}{\sin\theta_2} \tag{5.14}$$

$$A_2\left(\rho_{c2}, s_2^d\right) = \frac{1}{s_2^d}\sqrt{\frac{s_2^d\,\rho_0 \sin\alpha}{\rho_0 \sin\alpha - s_2^d \sin\theta_2}} \tag{5.15}$$

## 5.3 Calculation of diffraction coefficients

The dyadic diffraction coefficient [10] can be written as

$$\vec{D} = \begin{pmatrix} -D_s & 0 \\ 0 & -D_h \end{pmatrix} \tag{5.16}$$

with

$D_s$ the scalar diffraction coefficient for the soft boundary condition, which $\vec{\beta}_0^{\,i}$ converts to $\vec{\beta}_0^{\,d}$ ( see Fig. 5.5)

$D_h$ the scalar diffraction coefficient for the hard boundary condition, which $\vec{\phi}_0^{\,i}$ converts to $\vec{\phi}_0^{\,d}$ ( see Fig. 5.5)

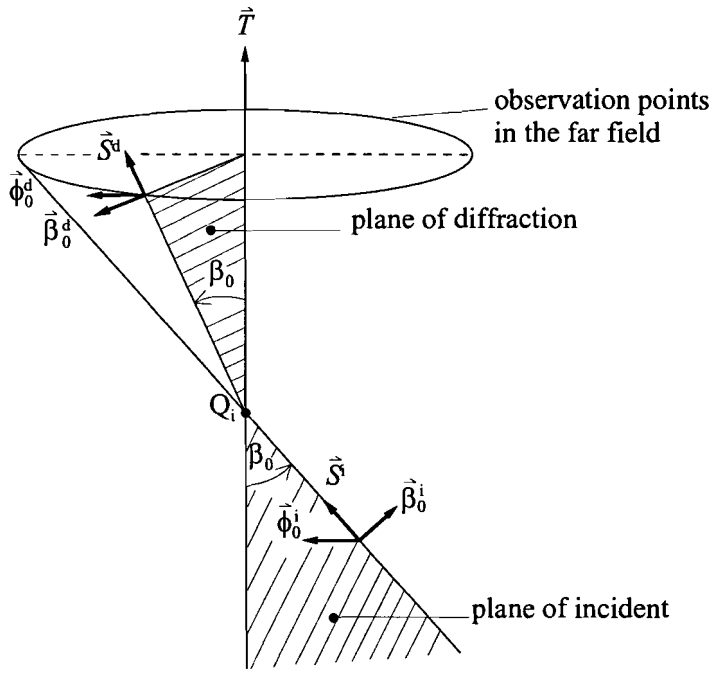


*Fig. 5.5: Diffraction at an edge*

The description of the unit vectors follows below:

$\vec{\phi}_0^{\,i}$ the unit vector perpendicular to the incident plane, which contains the vector $\vec{s}^{\,i}$ and the unit vector $\vec{T}$,

$\vec{\phi}_0^{\,d}$ the unit vector perpendicular to the diffraction plane, which contains the vector $\vec{s}^{\,d}$ and the unit vector $\vec{T}$,

$\vec{\beta}_0^{\,i}$ the unit vector parallel to the incident plane and related to the vector $\vec{s}^{\,i}$ and $\vec{\phi}_0^{\,i}$ by $\vec{\beta}_0^{\,i} = \vec{s}^{\,i} \times \vec{\phi}_0^{\,i}$ ,

$\vec{\beta}_0^{\,d}$ the unit vector parallel to the diffraction plane and related to the vector $\vec{s}^{\,d}$ and $\vec{\phi}_0^{\,d}$ by $\vec{\beta}_0^{\,d} = \vec{s}^{\,d} \times \vec{\phi}_0^{\,d}$ .

The diffraction coefficient $D_{\substack{s \\ h}}$ can generally be written in the following form [10]:

$$D_{\substack{s \\ h}} = \frac{-e^{-j\frac{\pi}{4}}}{2\sqrt{2\pi k}\sin\beta_0}\left\{\frac{F\left[kL^i\, a(r^d - r^i)\right]}{\cos\left(\frac{r^d - r^i}{2}\right)} \mp \frac{F\left[kL^i\, a(r^d + r^i)\right]}{\cos\left(\frac{r^d + r^i}{2}\right)}\right\} , \tag{5.17}$$

with

$r^i$ the angle between the incident ray and reflector surface tangent, which is perpendicular to the plane of incidence (see Fig. 5.3),

$r^d$ the angle between the diffraction ray and reflector surface tangent, which is perpendicular to the plane of diffraction.

$$F(z) = 2j\sqrt{z}\,\exp(jz)\int_{\sqrt{z}}^{\infty}\exp(-j\tau^2)d\tau \ , \tag{5.18}$$

involving a Fresnel integral.

The function F(z) will approach one if $z \to \infty$ (see Fig. 5.6).

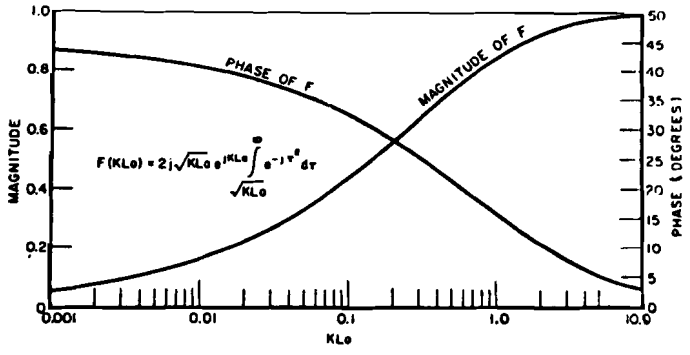


*Fig. 5.6 Modified Fresnel Transition function [10]*

$$a\left(r^d \mp r^i\right)=2\cos^2\left(\frac{r^d \mp r^i}{2}\right). \tag{5.19}$$

$L^i$ and $L^r$ denote the distance parameters defined as

$$L^i=\frac{s^d\left(\rho_e^i+s^d\right)\rho_1^i\rho_2^i\,\sin^2\beta_0}{\rho_e^i\left(\rho_1^i+s^d\right)\left(\rho_2^i+s^d\right)}, \tag{5.20}$$

$$L^r=\frac{s^d\left(\rho_e^r+s^d\right)\rho_1^r\rho_2^r\,\sin^2\beta_0}{\rho_e^r\left(\rho_1^r+s^d\right)\left(\rho_2^r+s^d\right)}. \tag{5.21}$$

$\rho_1^i$ and $\rho_2^i$ are the principal radii of curvature of the incident wavefront at $Q_i$.

$\rho_1^r$ and $\rho_2^r$ are the principal radii of curvature of the reflected wavefront at $Q_i$.

$\rho_e^r$ is given by

$$\frac{1}{\rho_e^r}=\frac{1}{\rho_e^i}-\frac{2\left(\vec{n}_{refl}\cdot\vec{n}\right)\cdot\left(\vec{s}^i\cdot\vec{n}_{refl}\right)}{\rho_g\sin^2\beta_0}, \tag{5.22}$$

with $\vec{n}_{refl}$ as the normal unit vector to the reflector surface at $Q_i$.

In the following section the diffraction coefficients for the reflector geometry under consideration will be derived.

## 5.3.1 *Diffraction coefficients for the upper diffraction point $Q_1$*

For the upper diffraction point $Q_1$ (see Fig. 5.3) the following expressions are valid:

$$\rho_e^i=\rho_0\,, \tag{5.23a}$$

$$\beta_0=\frac{\pi}{2}, \tag{5.23b}$$

$$\rho_1^i=\rho_2^i=\rho_0\,. \tag{5.23c}$$

Substitution of (5.23) in (5.20) yields a simplified expression for the $L^i$:

$$L^i = \frac{s_1^d \rho_0}{\rho_0 + s_1^d} . \tag{5.24}$$

From Fig. 5.3, the angles $r^i$ and $r^d$ for the upper diffraction point can be derived:

$$r_1^i = \frac{\pi}{2} - \alpha - \delta \ , \tag{5.25a}$$

$$r_1^d = \frac{3\pi}{2} - \delta - \theta_1 \ , \tag{5.25b}$$

with

$$\delta = -\tfrac{1}{2}\left[\alpha - \arctan\left(\frac{D_c - D}{6}\right)\right]. \tag{5.25c}$$

Hence,

$$\cos\left(\frac{r_1^d - r_1^i}{2}\right) = -\sin\left(\frac{\alpha - \theta_1}{2}\right) , \tag{5.26a}$$

$$\cos\left(\frac{r_1^d + r_1^i}{2}\right) = -\cos\left(\frac{2\delta + \alpha + \theta_1}{2}\right). \tag{5.26b}$$

Substitution of (5.26) in (5.19) yields the next two expressions:

$$a\left(r_1^d - r_1^i\right) = 2\sin^2\left(\frac{\alpha - \theta_1}{2}\right) \tag{5.27a}$$

$$a\left(r_1^d + r_1^i\right) = 2\cos^2\left(\frac{2\delta + \alpha + \theta_1}{2}\right) \tag{5.27b}$$

Now, the first transition function of the diffraction coefficient (5.17) is equal to

$$F\left[k L^i a\left(r^d - r^i\right)\right] = F\left[2k \frac{\rho_0 s_1^d}{\rho_0 + s_1^d} \sin^2\left(\frac{\alpha - \theta_1}{2}\right)\right] \tag{5.28}$$

with $k = \dfrac{2\pi}{\lambda}$.

To determine $\rho_e^r$ given in (5.22), we need the following expressions (see Fig. 5.3):

$$\vec{n}_{refl} \cdot \vec{n} = \sin\delta \ , \tag{5.29a}$$

$$\vec{s}_1^{\,i} \cdot \vec{n}_{refll} = -\cos(\alpha + \delta) \ , \tag{5.29b}$$

$$\rho_e^i = \rho_0 \ , \tag{5.29c}$$

$$\rho_g = \frac{D}{2} \ , \tag{5.29d}$$

$$\beta_0 = \frac{\pi}{2} \ . \tag{5.29e}$$

Substitution of (5.29) in (5.22) yields the expression for $\rho_e^r$ :

$$\rho_e^r = \frac{\rho_0 \, D}{D + 4\,\rho_0 \sin\delta \, \cos(\alpha + \delta)} \ . \tag{5.30}$$

The principal radius of curvature ' $\rho_1^r$ ' of the reflected wavefront at $Q_1$ (see Fig. 5.7) is equal to

$$\rho_1^r = \frac{D}{2\sin\left[\arctan\left(\frac{D_c - D}{6}\right)\right]} \ . \tag{5.31}$$

The principal radius of curvature ' $\rho_2^r$ ' of the reflected wavefront at $Q_1$ (see Fig. 5.8) is equal to

$$\rho_2^r = \sqrt{\left(\frac{D}{2} - x_s\right)^2 + y_s^2} \ . \tag{5.32}$$

This is the distance between the edge of the reflector and the intersection point of the reflected ray through the edge with the reflected ray that lies very close to it (see Fig. 5.8). The $(x_s, y_s)$ coordinates describes the intersection point.

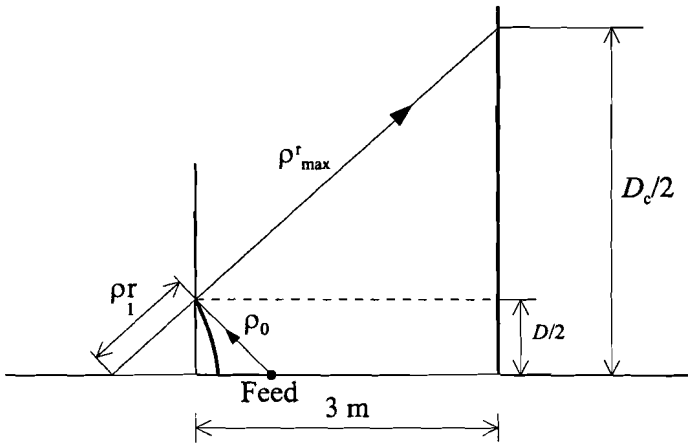


*Fig. 5.7: Incident and reflected rays through the edge*

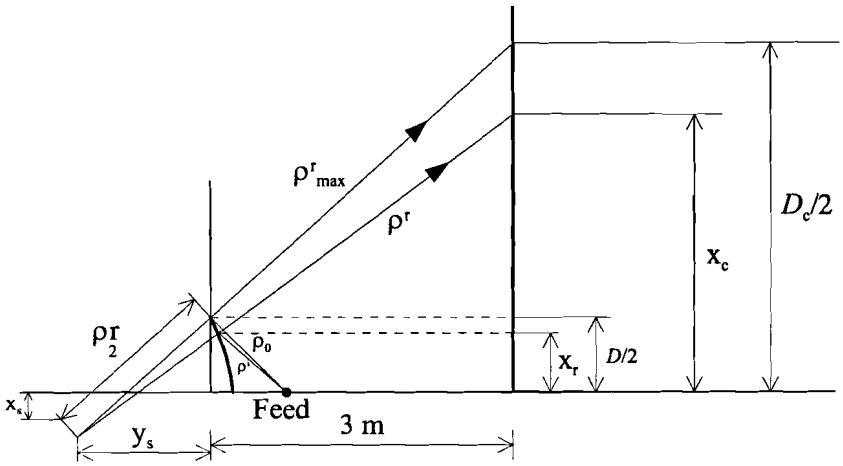


*Fig. 5.8: Incident and reflected rays through the edge and near to the edge*

Now, the $L^r$ be equal to

$$L^r = \frac{s_2^d\left(\rho_e^r + s_2^d\right)\rho_1^r\,\rho_2^r}{\rho_e^r\left(\rho_1^r + s_2^d\right)\left(\rho_2^r + s_2^d\right)}, \tag{5.33}$$

where $\rho_e^r$ , $\rho_1^r$ and $\rho_2^r$ are given in (5.30), (5.31) and (5.32) respectively.

The second transition function of the diffraction coefficient (5.17) is equal to

$$F\left[kL'a\left(r^d + r^i\right)\right] = F\left[2kL'\cos^2\left(\frac{\alpha + 2\delta + \theta_1}{2}\right)\right]. \tag{5.34}$$

Then, the scalar diffraction coefficient (5.17) becomes:

$$D_{\substack{s \\ h}} = \frac{e^{-j\frac{\pi}{4}}}{2\sqrt{2\pi\, k}}\left\{\frac{F\left[k\frac{\rho_0 s_1^d}{\rho_0 + s_1^d}\sin\left(\frac{\alpha - \theta_1}{2}\right)\right]}{\sin\left(\frac{\alpha - \theta_1}{2}\right)} \mp \frac{F\left[kL'\cos^2\left(\frac{\alpha + 2\delta + \theta_1}{2}\right)\right]}{\cos\left(\frac{\alpha + 2\delta + \theta_1}{2}\right)}\right\}. \tag{5.35}$$

Now, the vector property of the fields still have to be considered. This can be done by expressing the incident and diffracted fields in terms of two components according to the two orthogonal directions defined in Fig. 5.5. These are:

$$\vec{E}^i = E^i_{\beta_0}\,\vec{\beta}^i_0 + E^i_{\phi_0}\,\vec{\phi}^i_0, \tag{5.36a}$$

$$\vec{E}^d = E^d_{\beta_0}\,\vec{\beta}^d_0 + E^d_{\phi_0}\,\vec{\phi}^d_0. \tag{5.36b}$$

Inserting equation (5.36) in (5.2), and then comparing it with equation (5.16) shows that the relation between the incident fields and the diffracted fields can be written as:

$$\vec{E}^d(p) = \begin{pmatrix} E^d_{\beta_0} \\ E^d_{\phi_0} \end{pmatrix} = \begin{pmatrix} -D_s & 0 \\ 0 & -D_h \end{pmatrix}\begin{pmatrix} E^i_{\beta_0} \\ E^i_{\phi_0} \end{pmatrix}\frac{1}{s_1^d}\sqrt{\frac{s_1^d\,\rho_c}{\rho_c + s_1^d}}\; e^{-jks_1^d}. \tag{5.37}$$

For the symmetrical antenna configuration, the incident radiation from the feed is normal to the edge of the shaped reflector (see Fig. 5.5). So, $\beta_0$ equals $\pi/2$ and the directions of the different vectors can be shown as in Fig. 5.9, where the incident fields are projected on the plane (of incident) containing $\vec{s}^i$ and $\vec{T}$, and the diffracted fields from point $Q_i$ are projected on the plane (of diffraction) containing $\vec{s}^d$ and $\vec{T}$. Since these two planes generally do not coincide, the projection of all vectors onto the plane through the diffraction point $Q_i$ and perpendicular to the tangent $\vec{T}$ of the edge is drawn in Fig. 5.10.

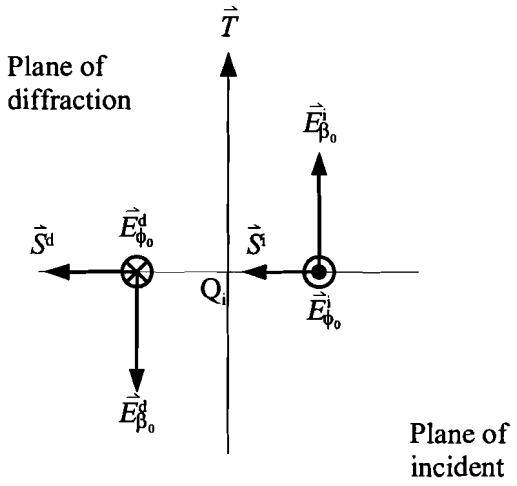


*Fig. 5.9: Diffraction at an edge (two dimensional in plane pararllel to $\vec{T}$ at $Q_i$)*

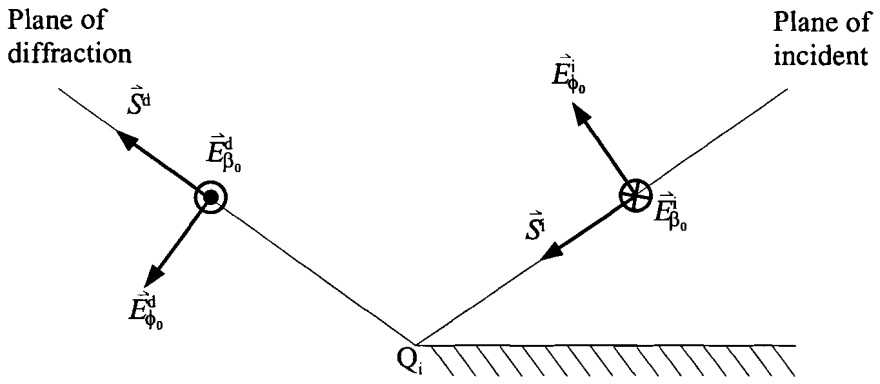


*Fig. 5.10: Diffraction at an edge (two dimensional in plane perpendicular to $\vec{T}$ at $Q_i$)*

Considering the diffraction point on the edge of the reflector, the following relations are found for the vector components of the incident and diffracted fields at the diffraction point $Q_1$ (Fig. 5.11):

$$E^d_{\phi_1} = -E^d_{\beta_{01}} , \tag{5.38a}$$

$$E^d_{\theta_1} = -E^d_{\phi_{01}} , \tag{5.38b}$$

$$E^i_{\beta_{01}} = E^i_{f\theta_1} , \tag{5.38c}$$

$$E^i_{\phi_{01}} = E^i_{f\theta_1} . \tag{5.38d}$$

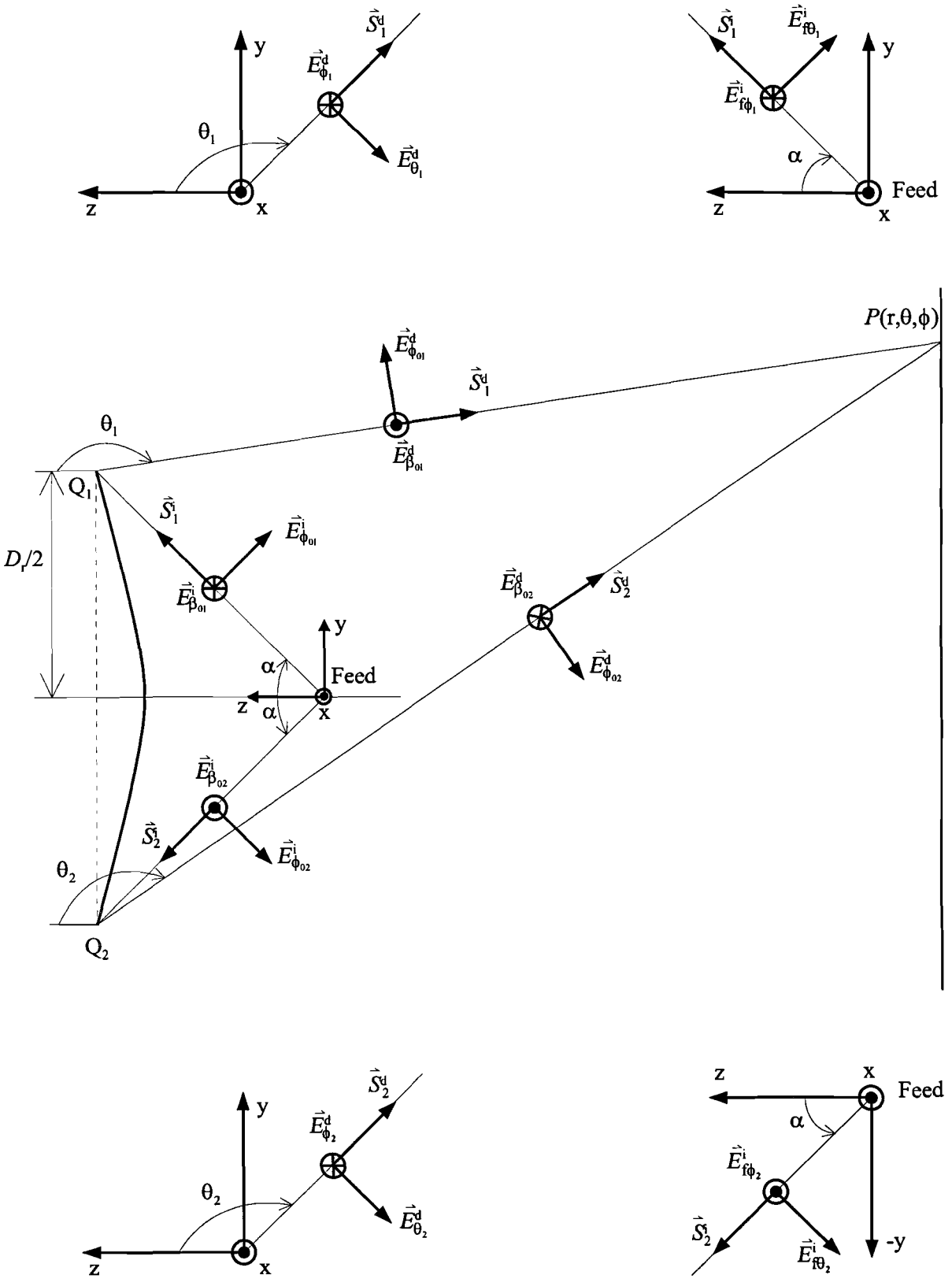


*Fig. 5.11: Diffraction at the shaped reflector [7]*

The dyadic diffraction field can be written as

$$\begin{pmatrix} E^d_{\phi_1} \\ E^d_{\theta_1} \end{pmatrix} = -\begin{pmatrix} E^d_{\beta_{01}} \\ E^d_{\phi_{01}} \end{pmatrix} = -\begin{pmatrix} -D_s & 0 \\ 0 & -D_h \end{pmatrix} \begin{pmatrix} E^i_{\beta_{01}} \\ E^i_{\phi_{01}} \end{pmatrix} \frac{1}{s_1^d} \sqrt{\frac{s_1^d \, \rho_{c1}}{\rho_{c1} + s_1^d}} \; e^{-jks_1^d}$$
$$= \begin{pmatrix} D_s & 0 \\ 0 & D_h \end{pmatrix} \begin{pmatrix} E^i_{f\Phi_1} \\ E^i_{f\Theta_1} \end{pmatrix} \frac{1}{s_1^d} \sqrt{\frac{s_1^d \, \rho_{c1}}{\rho_{c1} + s_1^d}} \; e^{-jks_1^d} \quad . \tag{5.39}$$

The incident field $\bar{E}_f(\rho_0, \alpha, \xi_1 = \phi)$ can be written in the form:

$$\begin{pmatrix} E^i_{f\Phi_1} \\ E^i_{f\Theta_1} \end{pmatrix} = A_0 \frac{e^{-jk\rho_0}}{\rho_0} \sqrt{G_f(\alpha)} \begin{pmatrix} \cos\phi \\ U_\alpha \sin\phi \end{pmatrix} , \tag{5.40a}$$

with

$$A_0 = \sqrt{Z_0 \frac{P_t}{2\pi}} , \tag{5.40b}$$

this is valid for a Huygens feed, where $P_t$ is the total power radiated by the feed and

$$Z_0 = 120\pi , \tag{5.40c}$$

is the intrinsic impedance of free space.

$$U_\alpha = 1 , \tag{5.40d}$$

is valid for a Huygens feed.

The feed power functions considered are:

$$G_f(\psi) = \begin{cases} 2(n+1)\cos^n(\psi) & (\psi \le \frac{\pi}{2}) \\ 0 & (\psi > \frac{\pi}{2}) \end{cases} , \tag{5.41}$$

where $n$ is a positive real.

Combining the equations (5.12), (5.35), (5.39) and (5.40) gives a general expression for the dyadic diffraction field valid for the shaped reflector.

$$\begin{pmatrix} E^d_{\phi_1} \\ E^d_{\theta_1} \end{pmatrix} = \frac{A_0}{2\rho_0 s_1^d} \left\{ \frac{F\left[k \frac{\rho_0 s_1^d}{\rho_0 + s_1^d} \sin^2\left(\frac{\alpha-\theta_1}{2}\right)\right]}{\sin\left(\frac{\alpha-\theta_1}{2}\right)} \mp \frac{F\left[k L' \cos^2\left(\frac{\alpha+2\delta+\theta_1}{2}\right)\right]}{\cos\left(\frac{\alpha+2\delta+\theta_1}{2}\right)} \right\}$$
$$\cdot \sqrt{\frac{G_f(\alpha) s_1^d \rho_0 \sin\alpha}{2\pi k\left(\rho_0 \sin\alpha + s_1^d \sin\theta_1\right)}} \begin{pmatrix} \cos\phi \\ U_\alpha \sin\phi \end{pmatrix} e^{-j\left(k\rho_0 + k s_1^d + \frac{\pi}{4}\right)} \tag{5.42}$$

If only a y-polarized incident field is considered and $\phi = \pi/2$, then both $E^i_{f\theta_1} = 0$ and $E^d_{\phi_1} = 0$. This leads to a diffraction field, equation (5.43), that contains only the scalar diffraction coefficient for the hard boundary '$D_h$' condition .

$$E^d_{\theta_1} = D_h E^i_{f\theta_1} \frac{1}{s_1^d} \sqrt{\frac{s_1^d \rho_{c1}}{\rho_{c1} + s_1^d}} e^{-jks_1^d} . \tag{5.43}$$

Now, the diffraction field for the y-polarized incident field is described by expression (5.44):

$$E^d_{\theta_1} = \frac{A_0}{2\rho_0 s_1^d} \left\{ \frac{F\left[2k \frac{\rho_0 s_1^d}{\rho_0 + s_1^d} \sin^2\left(\frac{\alpha-\theta_1}{2}\right)\right]}{\sin\left(\frac{\alpha-\theta_1}{2}\right)} + \frac{F\left[2kL_1' \cos^2\left(\frac{\alpha+2\delta+\theta_1}{2}\right)\right]}{\cos\left(\frac{\alpha+2\delta+\theta_1}{2}\right)} \right\}$$
$$\cdot \sqrt{\frac{G_f(\alpha) s_1^d \rho_0 \sin\alpha}{2\pi k\left(\rho_0 \sin\alpha + s_1^d \sin\theta_1\right)}} e^{-j\left(k\rho_0 + k s_1^d + \frac{\pi}{4}\right)} \tag{5.44}$$

## 5.3.2 *Diffraction coefficients for the lower diffraction point $Q_2$*

Proceeding similarly as in the previous section for $Q_2$, it is possible to find expressions for the angles $r^i$ and $r^d$ for the lower diffraction point (see Fig. 5.4). These are:

$$r_2^i = \frac{\pi}{2} - \alpha - \delta \ , \tag{5.45a}$$

$$r_2^d = -\frac{\pi}{2} - \delta + \theta_2 \ , \tag{5.45b}$$

Hence,

$$\cos\left(\frac{r_2^d - r_2^i}{2}\right) = \sin\left(\frac{\theta_2 + \alpha}{2}\right) , \tag{5.46a}$$

$$\cos\left(\frac{r_2^d + r_2^i}{2}\right) = \cos\left(\frac{\theta_2 - \alpha - 2\delta}{2}\right). \tag{5.46b}$$

Substitution of (5.44) in (5.19) yields the two expressions:

$$a\left(r_2^d - r_2^i\right) = \sin^2\left(\frac{\theta_2 + \alpha}{2}\right), \tag{5.47a}$$

$$a\left(r_2^d + r_2^i\right) = \cos^2\left(\frac{\theta_2 - \alpha - 2\delta}{2}\right). \tag{5.47b}$$

$L^i$ and $L^r$ for $Q_2$ are the same as (5.24) and (5.33) respectively.

Substitution of the equation (5.45), (5.46) and (5.47) into equation (5.17) yields expressions for the scalar diffraction coefficients for $Q_2$:

$$D_{\substack{s \\ h}} = \frac{-e^{-j\frac{\pi}{4}}}{2\sqrt{2\pi\, k}} \left\{ \frac{F\left[2k \frac{s_2^d \rho_0}{s_2^d + \rho_0} \sin^2\left(\frac{\theta_2 + \alpha}{2}\right)\right]}{\sin\left(\frac{\theta_2 + \alpha}{2}\right)} \mp \frac{F\left[2k\, L^r \cos^2\left(\frac{\theta_2 - \alpha - 2\delta}{2}\right)\right]}{\cos\left(\frac{\theta_2 - \alpha - 2\delta}{2}\right)} \right\}. \tag{5.48}$$

From Fig. 5.11, the following relations are found for the vector components of the incident and diffracted fields at the diffraction point $Q_2$:

$$E_{\phi_2}^d = E_{\beta_{02}}^d, \tag{5.49a}$$

$$E_{\theta_2}^d = E_{\phi_{02}}^d, \tag{5.49b}$$

$$E_{\beta_{02}}^i = E_{f\phi_2}^i, \tag{5.49c}$$

$$E_{\phi_{02}}^i = E_{f\theta_2}^i. \tag{5.49d}$$

The dyadic diffraction field for $Q_2$ can be written as

$$\begin{aligned}\begin{pmatrix} E^d_{\phi_2} \\ E^d_{\theta_2} \end{pmatrix} &= \begin{pmatrix} E^d_{\beta_{02}} \\ E^d_{\phi_{02}} \end{pmatrix} = \begin{pmatrix} -D_s & 0 \\ 0 & -D_h \end{pmatrix} \begin{pmatrix} E^i_{\beta_{02}} \\ E^i_{\phi_{02}} \end{pmatrix} \frac{1}{s_2^d} \sqrt{\frac{s_2^d \rho_{c2}}{(\rho_{c2} + s_2^d)}}\, e^{-jks_2^d} \\ &= \begin{pmatrix} -D_s & 0 \\ 0 & -D_h \end{pmatrix} \begin{pmatrix} E^i_{f\phi_2} \\ E^i_{f\theta_2} \end{pmatrix} \frac{1}{s_2^d} \sqrt{\frac{s_2^d \rho_{c2}}{\rho_{c2} + s_2^d}}\, e^{-jks_2^d} \end{aligned} \tag{5.50}$$

Writing $\vec{E}_f(\rho_0, \alpha, \xi_2 = \phi + \pi)$ at $Q_2$ in the form:

$$\begin{aligned}\begin{pmatrix} E^i_{f\phi_2} \\ E^i_{f\theta_2} \end{pmatrix} &= A_0 \frac{e^{-jk\rho_0}}{\rho_0} \sqrt{G_f(\alpha)} \begin{pmatrix} \cos(\phi + \pi) \\ U_\alpha \sin(\phi + \pi) \end{pmatrix} \\ &= A_0 \frac{e^{-jk\rho_0}}{\rho_0} \sqrt{G_f(\alpha)} \begin{pmatrix} -\cos(\phi) \\ -U_\alpha \sin(\phi) \end{pmatrix} \end{aligned}, \tag{5.51}$$

and combining the equations (5.15), (5.48), (5.50) and (5.51) gives a general expression for the diffraction field valid for $Q_2$.

$$\begin{aligned}\begin{pmatrix} E^d_{\phi_2} \\ E^d_{\theta_2} \end{pmatrix} = \frac{A_0}{2 s_2^d \rho_0} &\left\{ \frac{F\left[2k \frac{s_2^d \rho_0}{s_2^d + \rho_0} \sin^2\left(\frac{\theta_2 + \alpha}{2}\right)\right]}{\sin\left(\frac{\theta_2 + \alpha}{2}\right)} \mp \frac{F\left[2kL' \cos^2\left(\frac{\theta_2 - \alpha - 2\delta}{2}\right)\right]}{\cos\left(\frac{\theta_2 - \alpha - 2\delta}{2}\right)} \right\} \\ &\cdot \frac{1}{s_2^d} \sqrt{\frac{G_f(\alpha) s_2^d \rho_0 \sin\alpha}{2\pi\, k(\rho_0 \sin\alpha - s_2^d \sin\theta_2)}} \begin{pmatrix} \cos\phi \\ U_\alpha \sin\phi \end{pmatrix} e^{-j\left(k\rho_0 + k s_2^d - \frac{3\pi}{4}\right)} \end{aligned} \tag{5.52}$$

By taking $\phi = \pi/2$ and $U_\alpha = 1$ makes $E^i_{f\phi_2} = 0$, so that we have a diffraction field with only the diffraction coefficient for the hard boundary '$D_h$' condition.

$$E^d_{\theta_2} = -D_h E^i_{f\theta_2} \frac{1}{s_2^d} \sqrt{\frac{s_2^d \rho_{c2}}{\rho_{c2} + s_2^d}}\, e^{-jks_2^d} \tag{5.53}$$

By substituting the expression (5.48) for $D_h$ and (5.51) for $E^i_{f\theta_2}$ into (5.53), the diffracted field $E^d_{\theta_2}$ can be written as

$$E^d_{\theta_2} = \frac{A_0}{2\rho_0 s_2^d}\left\{\frac{F\left[2k\frac{\rho_0 s_2^d}{\rho_0+s_2^d}\sin^2\left(\frac{\alpha+\theta_2}{2}\right)\right]}{\sin\left(\frac{\alpha+\theta_2}{2}\right)} + \frac{F\left[2k\,L_2^r\cos^2\left(\frac{\theta_2-\alpha-2\delta}{2}\right)\right]}{\cos\left(\frac{\theta_2-\alpha-2\delta}{2}\right)}\right\} \cdot \sqrt{\frac{G_f(\alpha)\,s_2^d\,\rho_0\sin\alpha}{2\pi k(\rho_0\sin\alpha + s_2^d\sin\theta_2)}}\; e^{-j(k\rho_0+ks_2^d-\frac{3\pi}{4})} \tag{5.54}$$

## 5.4 *Total electric field*

The total electric field at the observation point $P$ is equal to the sum of the diffraction field originating from the two diffraction points $Q_1$, $Q_2$ and the reflected field. Assuming that there is an isotropic antenna placed in the observation point $P$, which is only sensitive for the θ-components of the incident fields. Then the voltage at the terminals of this antenna can be written as

$$V \propto c_1 E^d_{\theta_1} + c_2 E^d_{\theta_2} + E^r_{\theta_3} \tag{5.55}$$

The constants $c_1$ and $c_2$ are introduced because the reflected and diffracted fields are not normalized to the same power.

The normalized diffracted field on the coverage plane-section from $Q_1$ is equal to

$$E^{d1}(x_c) = E^d_{\theta_1}, \tag{5.56a}$$

the normalized diffracted field from $Q_2$ is equal to

$$E^{d2}(x_c) = E^d_{\theta_2}, \tag{5.56b}$$

and the normalized reflected field on the coverage plane-section is equal to

$$E^r(x_c) = E^r_{\theta_3}, \tag{5.56c}$$

where '$x_c$' is the variable along the coverage plane-section (-4 m ≤ $x_c$ ≤ 4 m).

Now, $V(x_c)$ can be written as

$$V(x_c) = E^r(x_c) + c_1 E^{d1}(x_c) + c_2 E^{d2}(x_c), \tag{5.57}$$

The value of $c_1$ and $c_2$ can be found by using the boundary conditions. At the edge ($x_c$ = 4 m) of the coverage plane-section, the following condition is valid:

$$c_1 E^{d1}(x_c = 4) = -\tfrac{1}{2} E^r(x_c = 4) \ . \tag{5.58a}$$

Hence,

$$c_1 = -\frac{E^r(x_c = 4)}{2E^{d1}(x_c = 4)} \ . \tag{5.58b}$$

At the edge ($x_c$ = -4 m) of the coverage plane-section, the following condition is valid:

$$c_2 E^{d2}(x_c = -4) = -\tfrac{1}{2} E^r(x_c = -4) \ . \tag{5.59a}$$

Hence,

$$c_2 = -\frac{E^r(x_c = -4)}{2E^{d2}(x_c = -4)} \ . \tag{5.59b}$$

Substitution of (5.58) and (5.59) into (5.57) yields an expression for the voltage:

$$V(x_c) \propto E^r(x_c) - \frac{E^r(x_c = 4)}{2E^{d1}(x_c = 4)} E^{d1}(x_c) - \frac{E^r(x_c = -4)}{2E^{d2}(x_c = -4)} E^{d2}(x_c) \ . \tag{5.60}$$

After normalizing the voltage $V(x_c)$ to the voltage due to the reflected field in the middle of the coverage plane-section $V^r(x_c=0)$, equation (5.60) can be expressed as (dB)

$$20 \log \left| \frac{V(x_c)}{V^r(x_c = 0)} \right| = 20 \log \left| \frac{E^r(x_c)}{E^r(x_c = 0)} - \frac{E^r(x_c = 4)}{2E^{d1}(x_c = 4)} \frac{E^{d1}(x_c)}{E^r(x_c = 0)} - \frac{E^r(x_c = -4)}{2E^{d2}(x_c = -4)} \frac{E^{d2}(x_c)}{E^r(x_c = 0)} \right| \tag{5.61}$$

The amplitude of the reflected field $\left|E^r(x_c)\right|$ on the coverage plane-section is equal to the root of the illumination function $H(x_c)$. So:

$$\left|E^r(x_c)\right| = \sqrt{H(x_c)} \ . \tag{5.62}$$

Because, the illumination function $H(x_c)$ is a constant and equals one, the amplitude of the reflected field $E^r(x_c)$ on the coverage plane-section is also a constant and equals one.

The reflected field on the coverage plane-section can be written as

$$E^r(x_c) = e^{-jk(\rho^i + \rho^r)} \ , \tag{5.63}$$

where $k(\rho^i + \rho^r)$ represents the phase of the field on the coverage plane-section, with $\rho^i$ and $\rho^r$ the length of the incident and reflected rays as given in (5.4) and (5.5), respectively, (see Fig. 5.2).

The total field on the coverage plane-section using the shaped reflector antenna with $F/D$=0.5, $D$=30 cm and the edge illumination from the feed of -10 dB, is given in Fig. 5.12

In Fig. 5.12, we can see that the maximum ripple of the field is about 1.5 dB. The field at the edge of the coverage plane-section attenuates to about -6 dB. This attenuation of the field at the edge of the coverage plane-section is unavoidable. The ripple of 1.5 dB can not be reduced by lowering the edge illumination from the feed or varying the *F/D*-ratio, because by changing one of these parameters, the reflector gets another shape. The diameter of the reflector is not going to change, because the diameter of 30 cm is chosen to be fixed.

In Fig. 5.13, the electric field on the coverage plane-section is given using the shaped reflector with *F/D*=0.5, *D*=30 cm and an edge illumination from the feed of -20 dB. This has maximum ripple of about 2.8 dB

In Fig. 5.14, the electric fields are given using the shaped reflectors with the following *F/D*-ratios: *F/D*=0.4 and *F/D*=0.6 with an edge illumination from the feed of -10 dB. For each other shaped reflector the electric field has a maximum ripple larger than 1 dB.

Lowering the edge illumination from the feed or varying the *F/D*-ratio do not result in reduction of the ripple.

These computations are unreliable around $x_c$=0. According to the equation of caustic divergence factor (5.12), there is a caustic at $x_c$=0. The UTD-method for the calculation of diffraction fails around $x_c$=0. In this region the well known method EEC (Equivalent Edge Current Calculation) must be applied for the calculation of diffraction. This is a θ-region (see Fig. 5.2) of about 3° [7, page 70]. This θ-region correspond with a $x_c$-region of ($-0.16 < x_c < 0.16$ m).

The conclusion that we can take from these computations, is that the total electric field using the reflector with *F/D*=0.4 and an edge illumination from the feed of -10 dB has the lowest ripple, but it is not low enough. To get an even lower ripple, a new reflector must be designed. This will be described in Chapter 6.

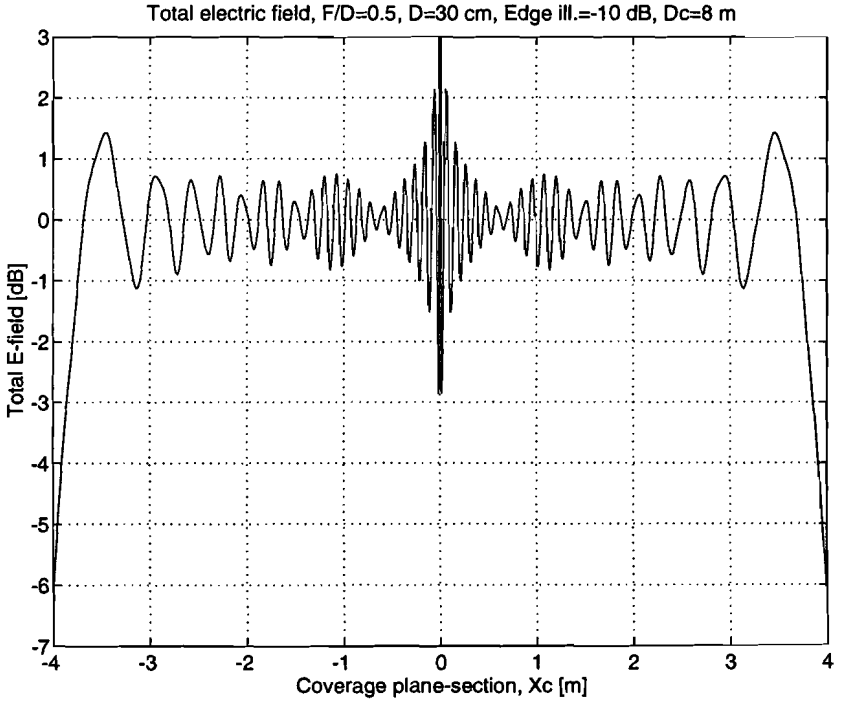


*Fig. 5.12: Total electric field on the coverage plane-section for a shaped reflector with F/D=0.5*

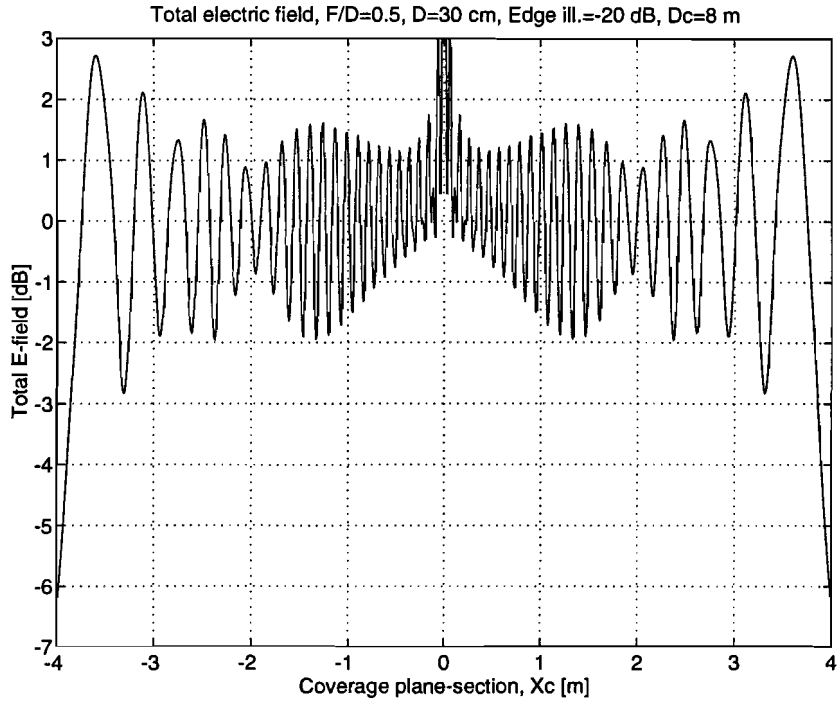


*Fig. 5.13: Total electric field on the coverage plane-section for a shaped reflector with edge illumination from the feed of -20 dB*

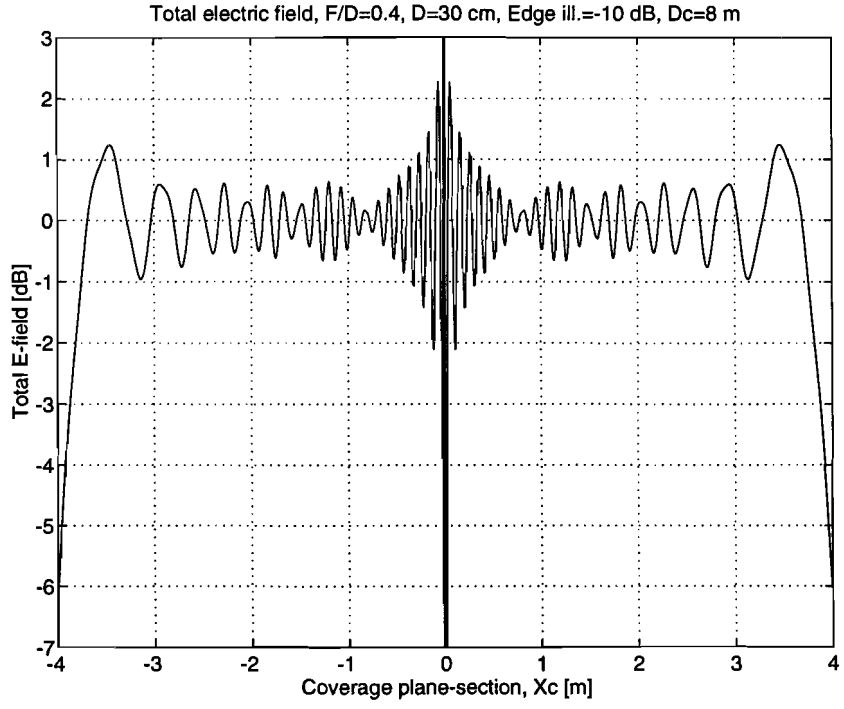


*Fig. 5.14a: Total electric field on the coverage plane-section for a shaped reflector with F/D=0.4*

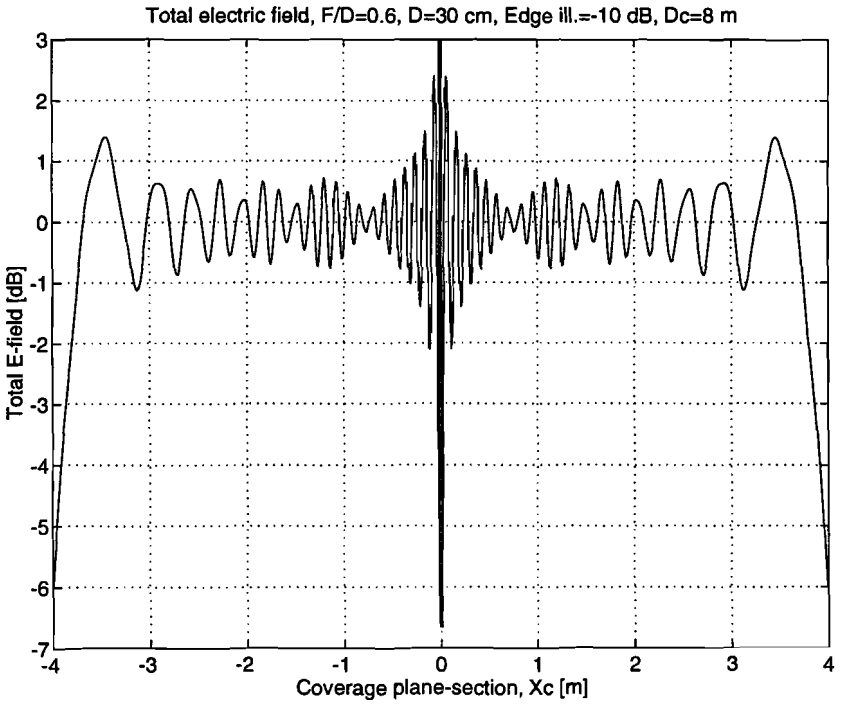


*Fig. 5.14b: Total electric field on the coverage plane-section for a shaped reflector with F/D=0.6*

# 6. Shaped reflector for extended coverage area

## 6.1 Design of the shaped reflector antenna

The ripple of the electric field within the coverage area with a diameter of 8 m can be reduced considerably by using a shaped reflector antenna dimensioned on a coverage plane-section of which the diameter is larger than 8 m, so that the maximum ripple will be found outside of the desired coverage area (this is the coverage plane-section with a diameter of 8 m). In our design, the diameter of the coverage area has been extended to 10 m. At the edge of the coverage plane, there is an attenuation larger than 6 dB, but this will also be found outside of the desired coverage area. The illumination function $H(x_c)$ on the coverage plane-section must be chosen so, that it is constant within the area with diameter of 8 m and outside of this it goes down. This has been done to make the ripple smaller.

The illumination function $H(x_c)$ is equal to

$$H(x_c)=\begin{cases}1 & \text{for} \quad 0\le x_c\le 4\\ 1-a(4-x_c)^2 & \text{for} \quad 4<x_c\le 5\end{cases}, \tag{6.1}$$

with '$a$' the slope of the function. Because $|E(x_c)|=\sqrt{1-a(4-x_c)^2}$, the slope must lie within the area: ($0 < a < 1$). Proceeding the design procedure of the reflector antenna as described in section 4.2, the reflector can be designed considering the illumination function $H(x_c)$ given in (6.1). Starting point is equation (4.8) in section 4.1.

$$\frac{\int_0^{x_c} H(r)\cos\left(\Psi^r(r)\right)r\,dr}{\int_0^{D_c/2} H(r)\cos\left(\Psi^r(r)\right)r\,dr}=\frac{\int_0^{\psi^i} G_f(\psi)\sin\psi\,d\psi}{\int_0^{\alpha} G_f(\psi)\sin\psi\,d\psi} \tag{4.8}$$

Equation (4.8) can be worked out for the different region.

For $0\le x_c\le 4$

$$\frac{\int_0^{x_c} H(r)\cos\left(\Psi^r(r)\right)r\,dr}{\int_0^{4} H(r)\cos\left(\Psi^r(r)\right)r\,dr+\int_4^{5} H(r)\cos\left(\Psi^r(r)\right)r\,dr}=\frac{\int_0^{\psi^i} G_f(\psi)\sin\psi\,d\psi}{\int_0^{\alpha} G_f(\psi)\sin\psi\,d\psi} \tag{6.2a}$$

For $4 \le x_c \le 5$

$$\frac{\int_0^4 H(r)\cos(\Psi^r(r))\,r\,dr + \int_0^{x_c} H(r)\cos(\Psi^r(r))\,r\,dr}{\int_0^4 H(r)\cos(\Psi^r(r))\,r\,dr + \int_4^5 H(r)\cos(\Psi^r(r))\,r\,dr} = \frac{\int_0^{\Psi^i} G_f(\psi)\sin\psi\,d\psi}{\int_0^{\alpha} G_f(\psi)\sin\psi\,d\psi} \qquad (6.2b)$$

with $D_c = 10$ m, $\Psi^i = \arctan\left(\frac{x_r}{F - y_r}\right)$, $\Psi^r = \arctan\left(\frac{x_c - x_r}{3 - y_r}\right)$ and $\alpha = \arctan\left(\frac{D}{2F}\right)$.

Substituting equation (6.1) in (6.2) yields the following solution:

For $0 \le x_c \le 4$:

$$\frac{\int_0^{x_c} \cos\left[\arctan\left(\frac{r-x_r}{3-y_r}\right)\right] r\,dr}{\int_0^4 \cos\left[\arctan\left(\frac{r-x_r}{3-y_r}\right)\right] r\,dr + \int_4^5 \cos\left[\arctan\left(\frac{r-x_r}{3-y_r}\right)\right]\left[1-a(4-r)^2\right] r\,dr} = \frac{\cos^{n+1}\left[\arctan\left(\frac{x_r}{b-y_r}\right)\right]-1}{\cos^{n+1}\left[\arctan\left(\frac{D}{2b}\right)\right]-1}, \qquad (6.3a)$$

For $4 < x_c \le 5$:

$$\frac{\int_0^4 \cos\left[\arctan\left(\frac{r-x_r}{3-y_r}\right)\right] r\,dr + \int_4^{x_c} \cos\left[\arctan\left(\frac{r-x_r}{3-y_r}\right)\right]\left[1-a(4-r)^2\right] r\,dr}{\int_0^4 \cos\left[\arctan\left(\frac{r-x_r}{3-y_r}\right)\right] r\,dr + \int_4^5 \cos\left[\arctan\left(\frac{r-x_r}{3-y_r}\right)\right]\left[1-a(4-r)^2\right] r\,dr} = \frac{\cos^{n+1}\left[\arctan\left(\frac{x_r}{b-y_r}\right)\right]-1}{\cos^{n+1}\left[\arctan\left(\frac{D}{2b}\right)\right]-1}. \qquad (6.3b)$$

Using 'Mathematica' [15], the integrals from (6.3) can be solved.

The integral, $Int1 = \int_4^{x_c} \cos\left[\arctan\left(\frac{r-x_r}{3-y_r}\right)\right]\left[1-a(4-r)^2\right] r\,dr$, from equation (6.3) has an analytical solution. This is:

$$Int1 = \frac{1}{6}|y_r - 3| \cdot \left\{ -\sqrt{25 - 8x_r + x_r^2 - 6y_r + y_r^2}\ \left[6 + a\left(4 + 52x_r - 11x_r^2 - 24y_r + 4y_r^2\right)\right] + \right.$$
$$+ \sqrt{9 + x_r^2 - 2x_r x_c + x_c^2 - 6y_r + y_r^2} \cdot$$
$$\left. \cdot \left[6 + a\left(-60 + 72x_r - 11x_r + 24x_c - 5x_r x_c - 2x_c^2 - 24y_r + 4y_r^2\right)\right] \right\} + \qquad (6.4)$$
$$+ \frac{1}{2}(y_r - 3)\left[2x_r + a\left(-72 - 5x_r + 16x_r^2 - 2x_r^3 + 48y_r - 18x_r y_r - 8y_r^2 + 3x_r y_r^2\right)\right] \cdot$$
$$\cdot \left\{ \operatorname{arcsinh}\left(\frac{x_c - x_r}{y_r - 3}\right) - \operatorname{arcsinh}\left(\frac{4 - x_r}{y_r - 3}\right) \right\}$$

The integral, $Int2 = \int_4^5 \cos\left[\arctan\left(\frac{r - x_r}{3 - y_r}\right)\right]\left[1 - a(4 - r)^2\right] r\, dr$, from equation (6.3) has a similar analytical solution with $x_c$=5. The solution of the integral, $Int3 = \int_0^{x_c} \cos\left[\arctan\left(\frac{r - x_r}{3 - y_r}\right)\right] r\, dr$, from (6.3) is given in equation (4.13). This is:

$$Int3 = |y_r - 3| \cdot \left(\sqrt{9 + x_r^2 - 2x_r x_c + x_c^2 - 6y_r + y_r^2} - \sqrt{9 + x_r^2 - 6y_r + y_r^2}\right) +$$
$$- (y_r - 3)\left(x_r\, arcsinh\left(\frac{x_c - x_r}{y_r - 3}\right) + x_r\, arcsinh\left(\frac{x_r}{y_r - 3}\right)\right) \qquad (6.5)$$

The integral, $Int4 = \int_0^4 \cos\left[\arctan\left(\frac{r - x_r}{3 - y_r}\right)\right] r\, dr$, from equation (6.3) has a similar analytical solution as the solution of *Int3* with $x_c$=4.

The shaped reflector antenna with *F/D*=0.5, D=30 cm, edge illumination from the feed = -10 dB and the boundary conditions:

$x_r = 0$ for $x_c = 0$,

$x_r = D/2$ and $y_r = 0$ for $x_c = 5$ m,

has the form as given in Fig. 6.1 for $a = 0.5$ and $a = 0.99$. In this figure, we can see that the reflector dimensioned for the illumination function with a slope near to one is less deep than that with a lower slope.

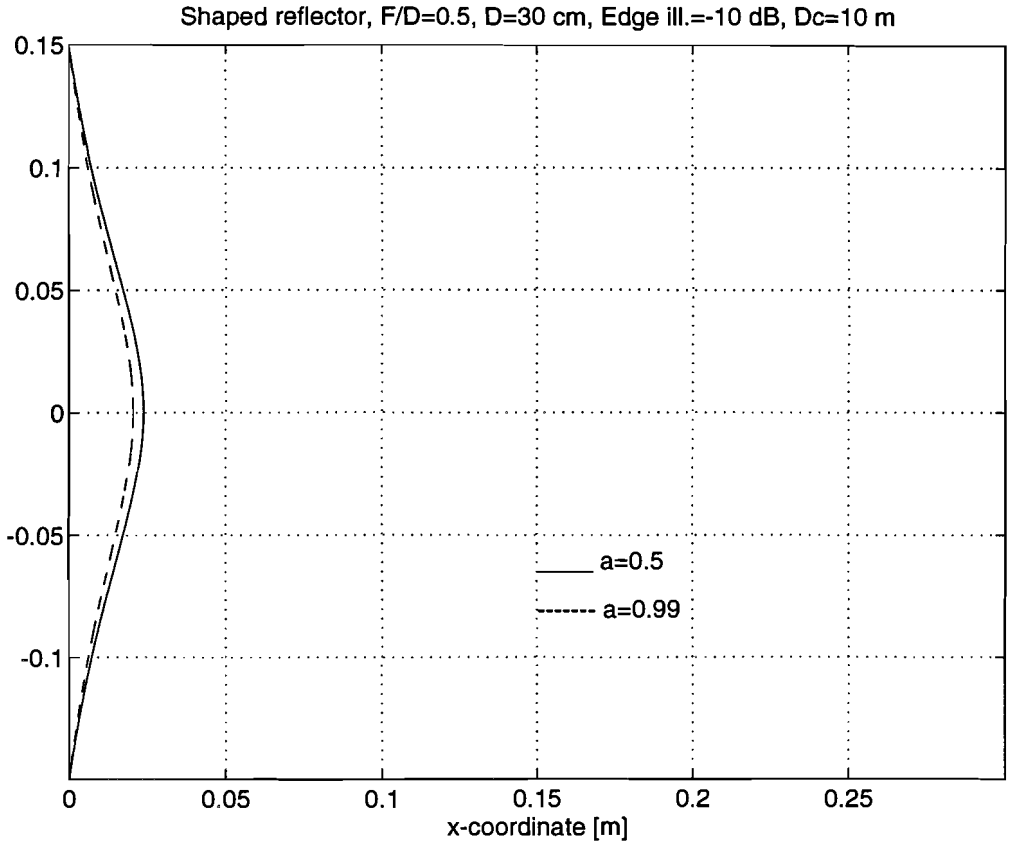


*Fig. 6.1: Shaped reflector for extended coverage plane-section*

In Fig. 6.2, the ray pattern of the shaped reflector is given where the slope '$a$' of the illumination function is equal to $a$=0.5. The angle between the rays from the feed is about 2°. Between the incident and reflected rays, the law of **Snel** is satisfied.

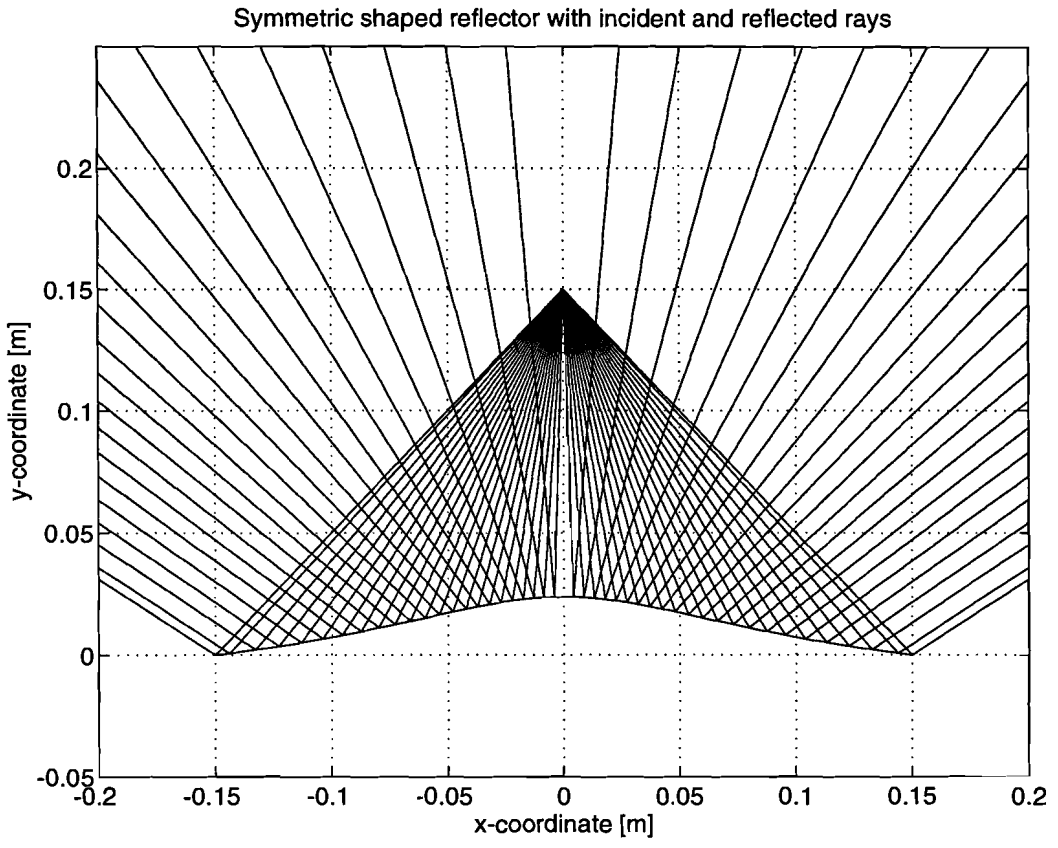


*Fig. 6.2: Ray pattern of the shaped reflector antenna for the extended coverage plane-section*

Ray pattern of the shaped reflector antenna with the following specification:

- Diameter of reflector $D$ = 30 cm
- $F/D$ = 0.5
- Edge illumination at feed = -10 dB
- Angle between the rays from feed = 2°
- Diameter of coverage plane-section = 10 m
- Illumination function on coverage plane-section: $H(x_c) = 1 - a(4 - x_c)^2$
- $a$ = 0.5

## 6.2 *Total electric field on extended coverage area*

The calculation of diffraction and total field on the extended coverage plane-section is based on the principle described in the previous section. In Fig. 6.3 , the total field is given for $a = 0.5$, $a = 0.9$ and $a = 0.99$. Assuming that there is an isotropic antenna placed in the observation point *P*, the voltage at the terminals can be written as

$$V(x_c) = E^r(x_c) + c_1 E^{d1}(x_c) + c_2 E^{d2}(x_c) \,, \tag{6.6}$$

with the boundary conditions:

$$c_1 E^{d1}(x_c = 5) = -\frac{1}{2} E^r(x_c = 5), \tag{6.7a}$$

and

$$c_2 E^{d2}(x_c = -5) = -\frac{1}{2} E^r(x_c = -5) \,. \tag{6.7b}$$

Substitution of (6.7) into (6.6) yields

$$V(x_c) = E^r(x_c) - \frac{E^r(x_c = 5)}{2E^{d1}(x_c = 5)} E^{d1}(x_c) - \frac{E^r(x_c = -5)}{2E^{d2}(x_c = -5)} E^{d2}(x_c) \,, \tag{6.8}$$

where the $E^r(x_c)$ for $(0 \le x_c \le 4)$ is equal to

$$E^r(x_c) = e^{-jk(\rho^i + \rho^r)}, \tag{6.9a}$$

and for $(4 < x_c \le 5)$

$$E^r(x_c) = \sqrt{1 - a\left(4 - x_c^2\right)}\; e^{-jk(\rho^i + \rho^r)}, \tag{6.9b}$$

with $\rho^i$ and $\rho^r$ given in (5.4) and (5.5) respectively. Normalizing equation (6.8) to the voltage due to the reflected field in the middle of coverage plane-section $V^r(x_c=0)$, the voltage can be written (in dB) as

$$20 \log \left| \frac{V(x_c)}{V^r(x_c = 0)} \right| = 20 \log \left| \frac{E^r(x_c)}{E^r(x_c = 0)} - \frac{E^r(x_c = 5)}{2E^{d1}(x_c = 5)} \frac{E^{d1}(x_c)}{E^r(x_c = 0)} - \frac{E^r(x_c = -5)}{2E^{d2}(x_c = -5)} \frac{E^{d2}(x_c)}{E^r(x_c = 0)} \right| \tag{6.10}$$

From Fig. 6.3, we can observe clearly that the attenuation much larger than 6 dB at the edge of the coverage plane-section and the maximum ripple appear outside the desired (coverage area with a diameter of 8 m). We can also observe that the highest value of the slope of the illumination function leads to the smallest diffraction.

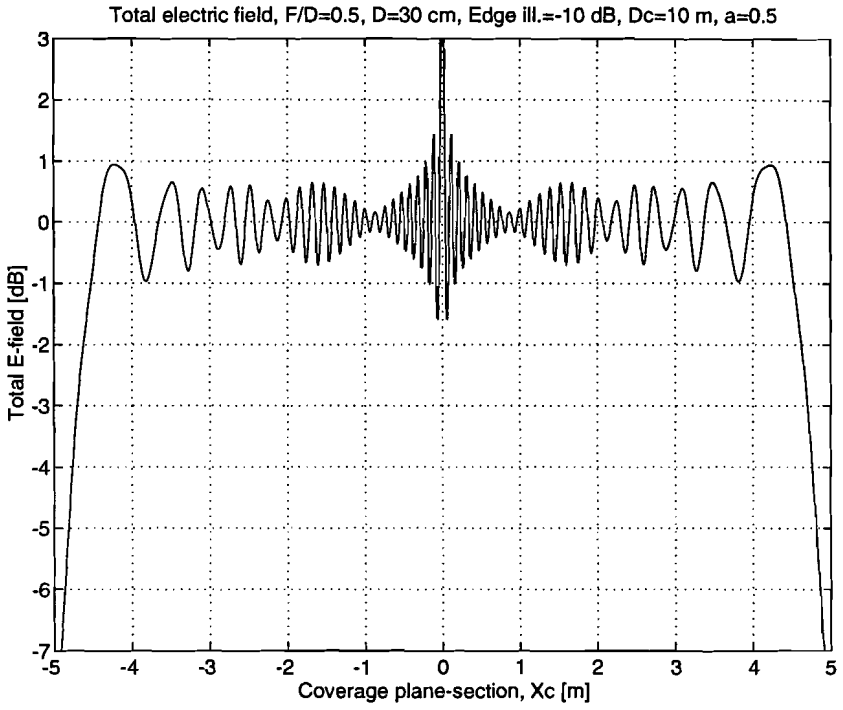


Fig. 6.3a: Total electrical field on the extended coverage plane-section where the illumination function has a slope of $a = 0.5$

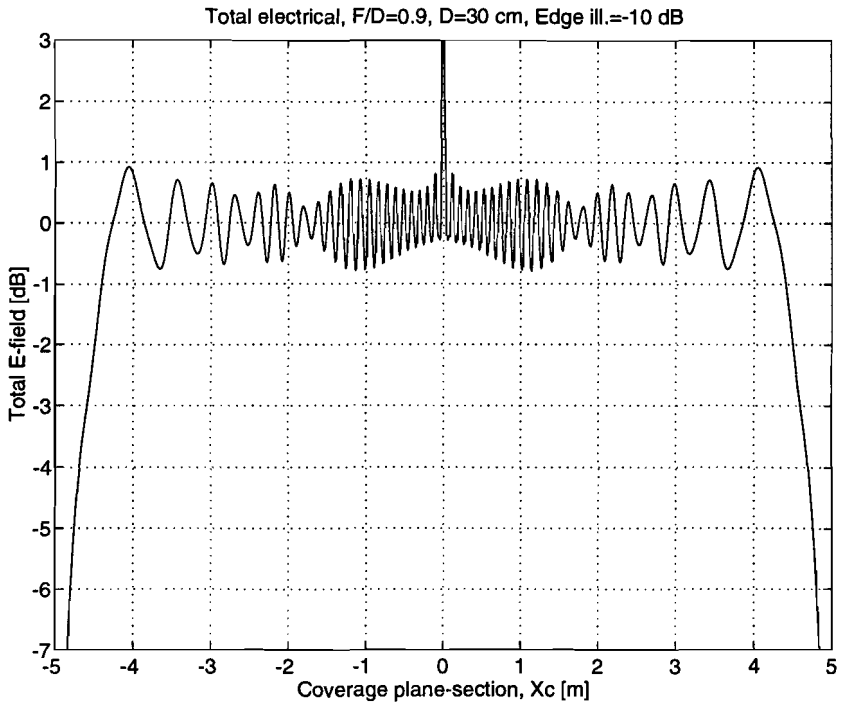


Fig. 6.3b: Total electrical field on the extended coverage plane-section where the illumination function has a slope of $a = 0.9$

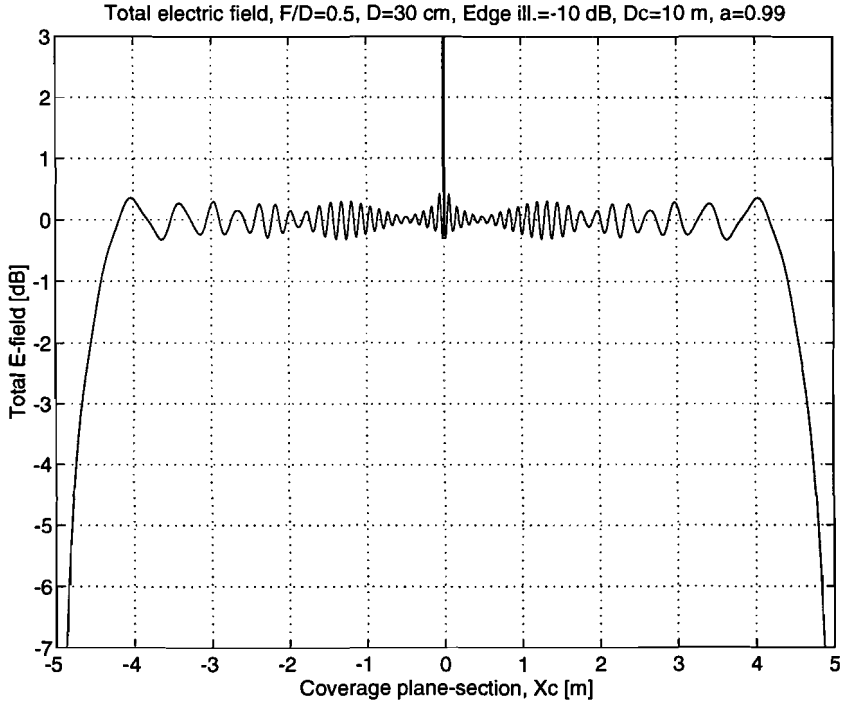


Fig. 6.3c: Total electrical field on the extended coverage plane-section where the illumination function has a slope of $a = 0.99$

# 7. Conclusions and Recommendations

## 7.1 Conclusions

Antennas for the (MSS) Median Server Station have been designed that will be used for the Median demonstrator. The demand that was made on the design was that the antenna, fixed at a height of 3 m, should exhibit an uniform coverage on the coverage plane-section (circle area on the ground with a diameter of 8 m).

The first antenna that has been designed is the bended biconical-horn antenna. This antenna derived from the standard biconical-horn antenna by bending it downwards. The performance of the bended biconical-horn antenna does not satisfy the demand of uniform coverage because it exhibits a ring-shaped coverage with a ring width of about 2 m. By increasing the angle of bending, the ring-shaped coverage area becomes narrower and it slides towards the centre of the coverage plane. This antenna can be used in special applications.

The second antenna that has been designed is the shaped reflector antenna with a diameter of 30 cm. The reflector is shaped in such a way that there arises always a uniform coverage on the coverage plane. Because of diffraction at the edges of the reflector, ripples appear in the field on the coverage plane. The maximum ripple is larger than 1.5 dB and there is an attenuation of 6 dB at the edge of the coverage plane-section. The ripple can not be reduced by varying the F/D-ratio or lowering the edge illumination at the feed, because by changing one of these parameters the reflector gets another shape. This problem has been solved by shaping the reflector for a coverage plane-section with a diameter larger than 8 m, so that the maximum ripple and the attenuation larger 6 dB at the edge of coverage plane-section will be found outside the desired coverage area. By taking a tapered illumination function on the coverage plane, a smaller ripple is realized. The maximum ripple was found to be smaller than 0.5 dB. So, we can conclude that the coverage of the shaped reflector antenna is almost uniform and it is therefore a suitable antenna for the Median demonstrator.

## 7.2 Recommendations

In the general introduction (Chapter 1), three types of antennas are mentioned that can be used for the Median demonstrator. The performances of the first two antenna types have been investigated and it was concluded that the shaped reflector is a suitable antenna for the Median demonstrator. It is recommended to analyze also the third type, i.e., corrugated-horn antenna and compare its performance with that of the shaped reflector antenna.

The second recommendation is to investigate the influence of blocking on the performance of the shaped reflector antenna. Another recommendation is to realize the shaped reflector with the appropriate parameters and verify its performance by measurements.

# *References*


[1] Smulders, Peter F. M. and Anthony G. Wagemans
Biconical horn antennas for near uniform coverage in indoor areas at mm-wave frequencies,
IEEE Trans. on Vehicular Technology, Vol. 43, no. 4, November 1994.

[2] Smulders, Peter F. M. and Anthony G. Wagemans
Millimetre-wave biconical-horn antennas for near uniform coverage in indoor pcio cells,
Electronics Letters, Vol. 28, no. 7, pp. 679-680, March 1992.

[3] Smulders, P. F. M.
Broadband wireless LAN's: A feasibility study,
EUT, The Netherlands, 1995, ISBN 90-386-0100-X.

[4] Galindo, V.
Design of dual-reflector antennas with arbitrary phase and amplitude distribution,
IEEE Trans. on Antennas and Propagation, Vol. AP-12, pp. 403-408, 1964.

[5] Stumpers, F. L. H. M., 1984,
The history, development and future of telecommunications in Europe,
IEEE Communications Magazine, 22, 84-95, 1984.

[6] Ginneken van, K. and W. Kortsmit, L. van Reij
Numerical Turbo Pascal library, TPNumlib,
Version 1, 1991.

[7] Chen, J. and P. J. I. de Maagt, M. H. A. J. Herben
Wide-angle radiation pattern calculation of Paraboloidal reflector antennas,
EUT Report 91-E-252, 1991, ISBN 90-6144-252-4.

[8] Melters, M. A. A. and P. F. M. Smulders
Development of a model for mm-wave propagation within a room of a building,
EUT, The Netherlands.

[9] James, G. L.
Geometrical theory of diffraction for electromagnetic waves.
London: Peter Peregrinus, 1976.

[10] Kouyoumjian, R. G. and P. H. Pathak
An uniform geometrical theory of diffraction for an edge in a perfectly conducting surface.
Proc. IEEE, Vol. 62 (1974), pp. 1448-1461.

[11] Keller, J.B.
Geometrical theory of diffraction.
Journal of the Optical Society of America, Vol. 52 (1962), pp. 116-130.

[12] Keller, J.B.
Diffraction by an aperture.
Journal of Applied Physics, Vol.28 (1957), pp. 426-444.

[15] Wolfram, S
Mathematica, A system for doing mathematics by computer,
second edition, Addison-Wesley Publishing Company.

[16] Lee, Shung-Wu and Mysore S. Sheshadri, Vahraz Jamnejad, Ray Mittra
Refraction at a curved dielectric interface: Geometrical Optics solution,
IEEE Trans. on microwave theory and techniques, Vol. MTT-30, no.1, 1982.

[17] Kot, J.S. and N. Nikolic, R. A. Sainati, T. S. Bird
Aspects of antenna design for indoor wireless millimetre-wave systems,
Journal of Electrical and Electronic Engineering, Australia-IE Aust & The IREE Society
Vol. 15, no. 2, 1995.

# *Appendix A*

## Derivation of expression (3.1) and (3.2).

$$\sin\theta \neq \frac{\Delta h}{r} \tag{A1}$$

$$\theta' = \alpha + \theta \tag{A2}$$

$$\sin\theta' = \sin(\alpha + \theta) = \frac{\Delta h}{r} \ . \tag{A3}$$

Substituting of

$$\sin(\alpha + \theta) = \sin\alpha\cos\theta + \cos\alpha\sin\theta$$

in (A3) yields

$$\sin\alpha\cos\theta + \cos\alpha\sin\theta = \frac{\Delta h}{r} \ . \tag{A4}$$

Dividing left and right of equation (A4) by $cos\theta$ gives

$$\sin\alpha + \cos\alpha\tan\theta = \frac{\Delta h}{r}\frac{1}{\cos\theta} \ ,$$

$$\cos\theta = \frac{\Delta h}{r}\left(\sin\alpha + \cos\alpha\tan\theta\right)^{-1} \ . \tag{A5}$$

With $\theta = \theta' - \alpha$ , equation (A5) becomes

$$\cos\theta = \frac{\Delta h}{r}\frac{1}{\sin\alpha + \cos\alpha\tan(\theta' - \alpha)} \ . \tag{A6}$$

Substituting of $\theta' = \arcsin(\frac{\Delta h}{r})$ in (A6) yields

$$\cos\theta = \frac{\Delta h}{r}\frac{1}{\sin\alpha + \cos\alpha\tan\left[\arcsin\left(\frac{\Delta h}{r}\right) - \alpha\right]} \ . \tag{A7}$$

$$\sin\alpha\cos\theta + \cos\alpha\sin\theta = \frac{\Delta h}{r} \tag{A4}$$

Dividing left and right of equation (A4) by *sin*θ gives

$$\cos\alpha + \frac{\sin\alpha}{\tan\theta} = \frac{\Delta h}{r}\frac{1}{\sin\theta} \quad ,$$

$$\sin\theta = \frac{\Delta h}{r}\frac{\tan\theta}{\cos\alpha\tan\theta + \sin\alpha} \quad . \tag{A8}$$

With $\theta = \theta' - \alpha$ , equation (A8) becomes

$$\sin\theta = \frac{\Delta h}{r}\frac{\tan(\theta' - \alpha)}{\cos\alpha\tan(\theta' - \alpha) + \sin\alpha} \quad . \tag{A9}$$

Substituting of $\theta' = \arcsin(\frac{\Delta h}{r})$ in (A9) yields

$$\sin\theta = \frac{\Delta h}{r}\frac{\tan\left[\arcsin(\frac{\Delta h}{r}) - \alpha\right]}{\cos\alpha\tan\left[\arcsin(\frac{\Delta h}{r}) - \alpha\right] + \sin\alpha} \quad . \tag{A10}$$